Space-based observational constraints for 1-D plume rise models

Maria Val Martín,[1,2] Ralph A. Kahn,[3] Jennifer A. Logan,[1] Ronan Paugam,[4] Martin Wooster,[4] and Charles Ichoku[3]

Abstract. We use a space-based plume height climatology derived from observations made by the Multi-angle Imaging SpectroRadiometer (MISR) instrument aboard the NASA Terra satellite to evaluate the ability of a plume-rise model currently embedded in several atmospheric chemical transport models (CTMs) to produce accurate smoke injection heights. We initialize the plume-rise model with assimilated meteorological fields from the NASA Goddard Earth Observing System and estimated fuel moisture content at the location and time of the MISR measurements. Fire properties that drive the plume-rise model are difficult to estimate and we test the model with four estimates for active fire area and four for total heat flux, obtained using empirical data and Moderate Resolution Imaging Spectroradiometer (MODIS) fire radiative power (FRP) thermal anomalies available for each MISR plume. We show that the model is not able to reproduce the plume heights observed by MISR over the range of conditions studied (maximum r^2 obtained in all configurations is 0.3). The model also fails to determine which plumes are in the free troposphere (according to MISR), key information needed for atmospheric models to simulate properly smoke dispersion. We conclude that embedding a plume-rise model using currently available fire constraints in large-scale atmospheric studies remains a difficult proposition. However, we demonstrate the degree to which the fire dynamical heat flux (related to active fire area and sensible heat flux), and atmospheric stability structure influence plume rise, although other factors less well constrained (*e.g.*, entrainment) may also be significant. Using atmospheric stability conditions, MODIS FRP, and MISR plume heights, we offer some constraints on the main physical factors that drive smoke plume rise. We find that smoke plumes reaching high altitudes are characterized by higher FRP and weaker atmospheric stability conditions than those at low altitude, which tend to remain confined below the BL, consistent with earlier results. We propose two simplified parameterizations for computing injection heights for fires in CTMs and discuss current challenges to representing plume injection heights in large scale atmospheric models.

1. Introduction

Biomass burning is a significant source of trace gases and aerosols to the atmosphere, with the potential to alter its chemical and radiation properties over extensive regions. Fires are also important sources of heat, which generates strong updrafts above the fire. The energy emitted by fires, in combination with atmospheric conditions, determines the vertical distribution of the fire emissions in the atmosphere near the fire source (*i.e.*, injection height). Global and regional chemical transport models (CTMs) have been used to study the impact of fire emissions on air quality and atmospheric composition [*e.g. Pfister et al., 2006; Turquety et al., 2007; Spracklen et al., 2007]*. Thus, knowledge of the injection heights is fundamental to accurately representing fire emissions in CTMs. However, representing injection heights in models is a difficult task, complicated by the sparseness of plume height measurements to validate the calculated values. The space-based plume height climatology derived from observations made by the Multi-angle Imaging SpectroRadiometer (MISR) instrument aboard the NASA Terra satellite provides a unique dataset for extensive validation of injection heights. We use these data to evaluate a one dimensional (1-D) plume-rise parameterization currently used to simulate injection heights in CTMs, and to investigate the main physical factors that determine smoke plume rise.

Fire emissions reach a wide range of altitudes in the atmosphere. Plume heights have commonly been measured for isolated fires on a case-by-case basis. For example, smoke plumes have been observed completely confined within the atmospheric boundary layer (BL) [*e.g. Trentmann et al., 2002]* and at different altitudes in the free troposphere (FT) (∼2 to 7 km) [*e.g. Wofsy et al., 1992; de Gouw et al., 2006]*. Wildfire plumes have also been detected within the lower stratosphere (>10 km) [*e.g. Fromm et al., 2005; Damoah et al., 2006; Dirksen et al., 2009]*, although this phenomenon occurs very sporadically and is associated with pyro-convective events triggered by intense heat from the fire and very unstable atmospheric conditions.

Recent advances in space-based observations have provided a tool for identifying smoke injection heights at regional-to-global scales. Smoke plume heights have been retrieved using space-borne lidar observations [*e.g. Labonne et al., 2007; Raffuse et al., 2012]*, stereo imaging [*e.g. Kahn et al., 2007, 2008; Val Martin et al., 2010; Mims et al., 2010; Tosca et al., 2011]* and aerosol index (AI) measurements [*Guan et al.*, 2010]. *Labonne et al.* [2007] studied

[1]School of Engineering and Applied Science, Harvard University, Cambridge, MA, USA.
[2]Now at Atmospheric Science Department, Colorado State University, Fort Collins, CO, USA.
[3]Climate & Radiation Laboratory, Code 613, NASA Goddard Space Flight Center, Greenbelt, MD, USA.
[4]King's College of London, Department of Geography, London, UK.

0148-0227/12/$9.00

hundreds of plumes distributed around the world using data from the Cloud-Aerosol Lidar with Orthogonal Polarization (CALIOP) on board the Cloud-Aerosol Lidar Infrared Pathfinder Satellite Observation (CALIPSO) satellite and found that smoke is mostly confined within the BL. In contrast, *Kahn et al.* [2008] found that, based on stereo-height retrievals from MISR, about 5–18% of the plumes reached the FT over Alaska and the Yukon territories in 2004 These results were supported by the comprehensive study of *Val Martin et al.* [2010], who analyzed about 3000 plumes across North America during 2002 and 2004–2007, and found that an important fraction (4–12%) of plumes inject smoke into the FT over North America. Following the case study analysis of *Kahn et al.* [2007], *Val Martin et al.* [2010] showed that smoke from the plumes reaching the FT typically get trapped within atmospheric stable layers, when they exist; otherwise smoke tends to spread-out vertically. A MISR 8-year plume height climatology for tropical forest and peatland fires over Borneo and Sumatra found that less than 4% of plumes reached the FT, suggesting that the direct injection of smoke into the free troposphere is not an important mechanism for vertical mixing of emissions over equatorial Asia [*Tosca et al.*, 2011].

In addition to MISR smoke plumes, *Val Martin et al.* [2010] also analyzed smoke clouds retrieved from MISR. Smoke clouds are smoke without a detectable fire origin and constitute a later stage of smoke plume evolution. This analysis showed that about 35% of smoke clouds reach the FT, a larger fraction than those of smoke plumes. The authors suggested that smoke from plumes may reach higher altitudes later in the day in part because fire intensity increases in the late afternoon, and in part because of atmospheric processes unrelated to the fire itself, such as convection and/or advection. High altitude plumes have also been detected using an empirical method based on AI from the Ozone Monitoring Instrument (OMI) and the Total Ozone Mapping Spectrometer (TOMS). *Guan et al.* [2010] identified 180 plumes above 8 km around the globe for a 10-year period. These findings are consistent with the previous documented detections of smoke in the free troposphere and lower stratosphere from isolated cases [*e.g. Fromm et al., 2005; Damoah et al., 2006; Dirksen et al., 2009].* However, it is important to note that these two studies are biased to dense high altitude smoke plumes, as dense smoke is easier to visualize by the MISR operator [*Val Martin et al.*, 2010] and to detect with the AI analysis [*Guan et al.*, 2010].

Smoke injection height is an important input in CTMs, as it has a strong influence on smoke dispersion [*e.g. Colarco et al., 2004].* Smoke lofted into the free troposphere is often transported hundreds or thousands of kilometers downwind because of the higher wind speeds at higher altitudes [*e.g. Val Martin et al., 2006; Dirksen et al., 2009]*, whereas smoke trapped within the boundary layer typically is well mixed and remains near the source region [*e.g. Trentmann et al., 2002].* Removal processes are also more efficient in the BL, whereas pollutants' lifetime increases when they are transported in the free troposphere [*Chatfield and Delany*, 1990]. At present, a wide range of arbitrary procedures is used to represent the vertical distribution of fire emissions in CTMs. Typically, a constant emission height is used. Emissions are either released initially within the BL [*e.g. Lamarque et al., 2003; Colarco et al., 2004]*, released at specified altitudes based on a simple empirical height-fire intensity relationship [*e.g. Lavoue et al., 2000; Wang et al., 2006]*, uniformly mixed throughout the troposphere [*e.g. Pfister et al., 2006]*, or a pre-selected fraction is released within and above the BL [*e.g. Leung et al., 2007; Turquety et al., 2007; Generoso et al., 2007; Hyer et al., 2007].* However, all these schemes neglect the effects of both the buoyancy generated by the fire and the atmospheric conditions, with the potential of introducing significant errors in CTM simulations.

Recently, more elaborate plume-rise parameterizations based on empirical and physical approaches have been incorporated into CTMs to take into account fire buoyancy and atmospheric conditions. Table 1 lists some of these parameterizations and the corresponding embedded CTM. For example, DAYSMOKE and Briggs are two empirical-statistical plume rise schemes [*Achtemeier et al.*, 2011; *Briggs*, 1969, respectively] embedded in the regional Community Multiscale Air Quality (CMAQ) model [*e.g. Liu et al., 2010; Achtemeier et al., 2011; Raffuse et al., 2012].* An evaluation of DAYSMOKE with six prescribed fires showed that the simulated injection heights were near the lower end of the range of observed plume heights. Similarly, *Raffuse et al.* [2012] found that simulated heights of smoke plume with the Briggs scheme were systematically lower than the values detected with MISR and CALIOP. The MISR-Briggs intercomparison also showed that modeled injection heights had much greater variability than the MISR heights, and the correlation between the two data sets was weak. These results suggest that accurately estimating plume heights with empirical schemes is a big challenge, since they relay on static meteorological conditions (e.g., wind speed and atmospheric stability), uncertain calculations of sensible heat and neglect the additional buoyancy generated by latent heat [*e.g. Raffuse et al., 2012; Liu et al., 2010; Stein et al., 2009].*

One of the most widely used parameterizations is the plume-rise model developed by *Freitas et al.* [2007], and recently modified to include the effect of horizontal winds [*Freitas et al.*, 2010]. The plume-rise model uses a prognostic scheme for simulating plume heights for tropical fires. The model determines fire buoyancy using the total sensible heat flux and area of each fire, and takes into account the additional buoyancy from latent heat. The plume-rise model was first embedded in the regional CATT-BRAMS model [*Freitas et al.*, 2007] and the global CAM model [*Guan et al.*, 2008] for exploratory case studies in the tropics. *Freitas et al.* [2007] demonstrated, using Atmospheric Infrared Sounder (AIRS) and aircraft observations, that explicitly accounting for injection processes significantly improves regional atmospheric model predictions of tropospheric CO across the central Amazon. At present, the validation of this plume-rise model has focused only on three case studies: the Quinault Fire described by *Trentmann et al.* [2002] [*Freitas et al.*, 2007] and two simulated fires with the 3-D Active Tracer High Resolution Atmospheric Model (ATHAM) [*Freitas et al.*, 2010].

More recently, the *Freitas et al.* [2007] plume-rise model has been embedded into WRF-Chem and used to study fires in North America [*Pfister et al.*, 2011; *Sessions et al.*, 2011; *Grell et al.*, 2011], using the heat fluxes and typical fire sizes for vegetation types in the tropics from *Freitas et al.* [2006]. *Sessions et al.* [2011] compared injection heights simulated by the WRF-Chem online plume-rise model to MISR heights obtained during the ARCTAS campaign over Siberia and Canada in 2008 and showed a poor correlation (r^2 <0.2) between the model and MISR plume heights. The authors also evaluated the long-range transport simulated by WRF-Chem with three injection height schemes (*i.e.*, plume-rise model, injected at 3–5 km and released within the BL). They found that the plume-rise model scheme produced the best match to AIRS observations, although the difference from results with the 3–5 km injection scheme was not significant. This underlines the complexities of representing plume injection heights in atmospheric models without compensating for errors within CTMs themselves, such as emissions and convective transport processes [*e.g. Chen et al., 2009; Hyer and Reid, 2009].*

In this work, we evaluate the plume-rise model described by *Freitas et al.* [2007, 2010] using the MISR plume height climatology presented in *Val Martin et al.* [2010]. We first develop a set of approaches to determine the fire characteristics needed to initialize the model (i.e., active fire area and

total heat flux). We also use the MISR plume heights, in combination with assimilated meteorological fields from the NASA Goddard Earth Observing System (GEOS) and Moderate Resolution Imaging Spectroradiometer (MODIS) fire radiative power thermal anomalies available for each MISR plume, to constrain smoke plume rise, independently of the plume-rise model. On the basis of these results, we recommend how to treat injection heights in CTMs and discuss current limitations and challenges to representing plume injection heights in large-scale atmospheric studies.

2. Data and methods

2.1. Aerosol smoke plume observations

We use observations of near-source plume heights over North America for the 2002 and 2004-2007 fire seasons, obtained with the MISR instrument. The plume height dataset was developed with the MISR Interactive eXplorer (MINX) software package (http://www.openchannelfoundation.org/projects/MINX). To retrieve smoke plume heights, MINX first locates fires in the MISR field of view using MODIS fire pixels and an operator then identifies the source and digitizes the boundaries of the plumes and determines the plume direction of transport. In addition to smoke plume heights, MINX also retrieves wind speeds and albedos, and provides aerosol properties (e.g., Angstrom exponent) from the MISR standard aerosol product, and total fire radiative power (FRP) and brightness temperatures from the MODIS thermal anomaly product [*Nelson et al.*, 2008a]. Each smoke plume height retrieval is assigned a flag that describes the quality of the digitization output (i.e., "good", "fair" or "poor") [*Nelson et al.*, 2008b]. The MINX plume data are publicly available at http://www-misr.jpl.nasa.gov/getData/accessData/MisrMinxPlumes/index.cfm. A detailed analysis of this climatology was presented in *Val Martin et al.* [2010].

Plume-rise models typically provide a maximum injection height above the fire, as described in section 2.2. A number of statistics are used to describe the heights of MISR plumes, such as the median, mode and maximum of the vertical distribution of the stereo-height retrievals [*e.g. Kahn et al., 2008; Val Martin et al., 2010; Tosca et al., 2011]*. In this work, we use plumes with a data quality flag of "good" and modify the definition of plume height derived from MISR to be compatible with that simulated by 1-D plume-rise models. We define the MISR plume height as the maximum of the stereo-height retrievals immediately above the fire source, whereas the heights in our previous work were aggregated over the entire plume. We take the fire source to be the area formed by the MODIS fire pixels clustered at the origin of the fire plume, and include a buffer around this cluster of 10% of the cluster radius. Following the quality protocol established for plumes digitized by MINX [*Nelson et al.*, 2008a], we limit cloud contamination by setting the maximum height as the 99th percentile of the smoke pixels retrieved above the fire source. In addition, only plumes having more than five smoke retrievals above the fire source are considered. To characterize the fires associated with each plume, and to select cases with well-defined fires, we consider only those plumes having MODIS fire pixels clustered at the plume origin. We also exclude from the analysis pixels that are located more than 2 km away from the cluster. These additional constraints removed 62% of the good quality plumes in the dataset studied by *Val Martin et al.* [2010], leaving a total sample size of 835 plumes.

Figures 1a and 1b compare the vertical distributions of stereo-height pixels provided by the MISR dataset, and the stereo-height pixels that we consider to be above the fire source. The modification of the plume height definition does not significantly change the plume height analysis of *Val Martin et al.* [2010], it simply provides a more appropriate comparison between MISR-derived plume heights and model injection heights. For example, with the new definition, the plume in Figure 1a has a best estimated maximum height above ground level of 3150 m and a total fire radiative power of 2100 MW, whereas these parameters are 3325 m and 2325 MW for the entire plume, used in the original dataset. For analysis purposes, a plume altitude of 3150 m above the fire source is more representative of a modeled injection height, as it does not take into account atmospheric processes unrelated to the fire itself that may affect the final plume rise; a total FRP of 2100 MW gives an estimate of the fire radiative heat output for a well-defined fire, and avoids including in the analysis fire pixels from areas burning near the plume origin, which the model cannot simulate.

2.2. Plume-rise model

We evaluate the 1-D plume-rise model described by *Freitas et al.* [2007] and *Freitas et al.* [2010]. This plume-rise parameterization scheme was originally developed by *Latham* [1994], and assumes that smoke and trace gases are transported upward due to positive buoyancy produced by the fire. The altitude reached by these emissions is a complex function of fire energy and local meteorology at the time of burning. Within the column above the fire there is a decrease in temperature due to radiative cooling, and efficient heat transport by convection. In addition, the plume dilutes and loses buoyancy due to entrainment of colder environmental air into the smoke plume, and lateral entrainment due to the drag of the wind. An additional positive buoyancy is sometimes generated from latent heat, when water vapor condenses [*Freitas et al.*, 2007]. The 1-D plume-rise model accounts for these processes, and is governed by equations based on energy conservation, vertical momentum conservation, and continuity of water phases [*Freitas et al.*, 2007, 2010]. The final height of the plume (i.e., the top of the plume or "injection height") is determined as the height at which the vertical velocity of the air parcel is less than 1 m/s [*Freitas et al.*, 2006]. Figures 1c and 1d show three output parameters estimated by the model (plume vertical velocity, vertical mass distribution and acceleration buoyancy) at the locations of two MISR plumes, one high-altitude plume observed in central Canada in 2005 and one low-altitude plume observed in Texas in 2006. In these cases, the model predicts that the vertical velocities of the simulated plumes diminish with altitude, and the plumes reach maximum heights above ground level (agl) of 3500 m and 850 m, respectively, similar to those observed by MISR for the actual plumes (3150 m and 596 m).

2.3. Input data for plume-rise model

The plume-rise model is driven by four main inputs: active fire area, total fire heat flux, fuel moisture content of the burning vegetation, and meteorological variables (i.e., relative humidity (RH) , temperature and wind speed profiles), as discussed by *Freitas et al.* [2007]. The model calculates the buoyancy flux generated by the fire using the sensible heat flux, assumed to be 55% of the total fire heat flux, and the radius of the plume, which is estimated from the active fire size. Typically, the 1-D plume model is embedded in each column of a 3-D host model, in which the 3-D model feeds the plume model the environmental parameters [*e.g. Freitas et al., 2007; Pfister et al., 2011; Sessions et al., 2011]*. In this work, we run the plume-rise model at the location of the MISR plumes, independently of a 3-D model. We initialize the model with assimilated GEOS meteorological observations, and estimate the fuel moisture content using the Canadian Fire Weather Index (FWI) system [*Van Wagner*, 1987] at the location and time of the MISR plume observations. Additionally, we used several approaches to

determine the active fire area and the total heat flux for the MISR plume fires. These parameters are difficult to estimate, and large uncertainties exist in the data currently available [*e.g. Hyer and Reid, 2009; Schroeder et al., 2010]*. We discuss them separately in section 2.4.

For meteorological conditions, following the work of *Val Martin et al.* [2010], we used the GEOS meteorological fields that were archived for running the GEOS-Chem global model, with degraded resolution of 2° latitude by 2.5° longitude. The temporal resolution of the fields is 6 hours (3 hours for surface variables and mixing depths). We extracted RH, temperature and wind speed data from GEOS-4 for 2002 and 2004–2006, and GEOS-5 for 2007. GEOS-4 has 55 vertical levels between the surface and 0.01 hPa (including 5 levels up to 2 km), whereas GEOS-5 has 72 vertical levels, with 14 levels up to 2 km. Due to the difference between the horizontal resolution of GEOS and MISR (200 km versus 1.1 km), there was in some cases a mismatch between the terrain elevations. To avoid a bias in the results due to the terrain difference, we excluded the observations for which the difference between the MISR and GEOS terrain elevation exceeded 250 m. This resulted in the removal of about 30% of the plume cases, leaving a total of 584 plumes. In addition, to assess the relationship between the injection height given by the model and the atmospheric structure, we used the atmospheric boundary layer heights provided with the GEOS fields [*Lucchesi*, 2007].

Vegetation fuel moisture content at the fire locations was estimated as the average of the fine fuel and duff moisture content, obtained from the Fine Fuel Moisture Code (FFMC) and the Duff Moisture Code (DMC), respectively, and calculated using surface meteorological observations with the FWI system. Typical fuel moisture content at the location of the MISR plumes was 40.3% (reported median of all observations), which is similar to the 40% employed by *Trentmann et al.* [2006] for an extra-tropical forest fire simulation. The fuel moisture values used here are somewhat larger than the 10% used as default in the plume-rise model. However, we found that the injection height results are not particularly sensitive to the fuel moisture content.

2.4. Fire buoyancy configurations

To evaluate the performance of the plume rise model relative to the fire buoyancy sources, we tested four approaches for determining the total heat flux and four for the active fire area. Table 2 summarizes the 16 possible configurations.

2.4.1. Total Heat flux

The approaches for total heat flux from the fires are named FT06, FUEL, Dual-Band and FRPx10, as shown in Table 2. A summary of the heat flux values estimated using these approaches is presented in Table 3.

Freitas et al. [2006] adopted upper and lower limit heat flux values for three types of vegetation in Brazil (grassland, woody savanna, and tropical forest), based on the fire literature for that region. For our FT06 approach, we classify vegetation in three groups: grassland, shrubland and forest, and use the values in *Freitas et al.* [2006], as these were adopted in previous modeling work for the extratropics [*e.g. Pfister et al., 2011; Sessions et al., 2011; Grell et al., 2011]*. We run the plume-rise model with the upper and lower limit values and report the average of the results, with the exception of grassland, for which only one value is given in *Freitas et al.* [2006].

The FRP approach is based on the fire radiative power reported for each fire pixel within the MISR plume dataset. Previous studies determined that fire radiative energy is about 10–20% of the total fire heat energy, based on the heat content of the fuels, and measurements of fire brightness temperature and spectral emittance [*Wooster et al.*, 2005; *Freeborn et al.*, 2008]. We thus consider the total heat flux released in each fire as the total FRP measured in each plume multiplied by 10. It is important to note that the MISR plume database provides the FRP values in MW. However, we consider the MODIS FRP as MW per 1 km pixel (thus in units of W/m^2). This assumption is appropriate in our analysis because the narrower MISR swath lies in the center of the MODIS/Terra swath. Thus, MODIS pixels are distorted very little near the center where MISR observes. The maximum correction to adjust the area to the scan angle applied to the MODIS pixels is 15% and this angle correction is used in a small fraction of the data [David Nelson, JPL, personal communication].

The Dual-Band approach is based on an implementation of the *Dozier* [1981] bi-spectral algorithm applied to the original MODIS Level 1B calibrated radiance data (MOD021km). Fire pixels within the MOD021km granules are first detected with an active fire detection algorithm that has been designed for use with the forthcoming Sentinel-3 Sea and Land Surface Temperature Radiometer (SLSTR), and whose performance has been recently evaluated using MODIS and ASTER data [*Wooster et al.*, 2012]. Each detected fire pixel from the MOD021km granule is assigned to a particular "fire", based on the analysis of clusters of spatially contiguous fire pixels. This is an approach similar to that used previously with data from the BIRD Hotspot Recognition Sensor [*Wooster et al.*, 2003; *Zhukov et al.*, 2005], and designed to minimize some of the problems of the dual band method, for example those related to inter-channel spatial misregistration effects [*Zhukov et al.*, 2005]. Each fire cluster is then subject to analysis using the *Dozier* [1981] "dualband" approach, using the specific method taken by *Zhukov et al.* [2005]. The output for each cluster is an estimate of the effective active fire temperature and active fire area, based on the fire clusters signals in the MODIS MIR and LWIR spectral bands, along with an estimate of the clusters total FRP. As in the FRP approach, we consider the total heat flux released in each fire as the total FRP multiplied by 10.

Our last approach uses fuel consumption to estimate the heat flux. We use an improved fuel consumption map for western North America [*Spracklen et al.*, 2009], and our own estimates for boreal North America. A description of the fuel consumption map is found in Appendix A. We refer to this approach as FUEL. We obtain heat flux values (i.e., W/m^2) from fuel consumption (i.e., kg/m^2) by assuming that the average burning time of the fire is two hours, and using a standard heat of combustion for extra-tropical vegetation of 18.7e6 J/Kg [*Trentmann et al.*, 2006].

2.4.2. Active fire area

We apply four approaches to estimating active fire area for each plume, based on MODIS data available for each MISR plume. It is well recognized that a simple count of fire pixels at the nominal 1-km MODIS resolution tends to vastly overestimate the active fire area [*e.g. Giglio et al., 2006]*. Our goal is therefore to retrieve fire areas at the sub-pixel level. Table 3 summarizes the statistical parameters for active fire areas by vegetation type obtained in each approach.

The first two approaches, WRF-Pxl and FLAMBE-Pxl, are based simply on the number of MODIS fire pixels, and differ only in the area assigned to each pixel. The WRF-Pxl approach clusters the pixels within each plume, assuming that the mean area burned within each fire pixel is 0.5 km^2. This assumption is used in the WRF-Chem online plume-rise configuration [Gabriele Pfister, NCAR, personal communication]. In WRF-Chem, fire pixels are aggregated within each model grid box (*e.g.*, 12x12 km in *Pfister et al.* [2011]). The FLAMBE-Pxl configuration is based on the Fire Locating and Modeling of Biomass Burning Emissions (FLAMBE) dataset [*Reid et al.*, 2009]. FLAMBE provides

carbon and aerosol emissions at hourly intervals, based on the WF-ABBA and MODIS active fire products. It simulates diurnal variability of emissions and reports burned area taking into account the diurnal variability of fires. For a 1 km MODIS fire pixel, FLAMBE assumes 0.625 km is burned, and partitions it into 24 hourly segments (i.e., 0 km for nighttime hours, 0.05 km for daytime hours and 0.025 km for transitions hours) [Edward Hyer, NRL, personal communication]. We therefore consider that, at the time of the MISR observations (11:00-14:00 local time over North America), 0.05 km on average is burning within each fire pixel. We then sum all fire pixels within each plume. The WRF-Pxl approach returns active fire areas that are exactly a factor of 10 larger than the FLAMBE-Pxl approach, as shown in Table 3.

The third approach, scaled-FRP, is based on the FRP data reported for each fire pixel. We assume that the pixel with the maximum MODIS FRP value ever detected within each biome burns completely (i.e., active fire area for that pixel equaled 1 km^2). We then scale the rest of the MODIS FRP values by this maximum and sum those resulting fractional areas to obtain total active fire area for each plume. For example, the maximum FRP value detected over the boreal forest is 1710 W/m^2. Thus, an FRP of 800 W/m^2 within the same type of vegetation is assigned an active fire area of 0.47 km^2. Finally, the Dual-Band approach estimates the active fire area using the bi-spectral method of *Dozier* [1981] applied to the individual fire clusters.

As shown in Table 3, these four approaches provide the model with active fire areas that differ significantly, with a range factor of 50–100. For example, the WRF-Pxl is about 10 times the FLAMBE-Pxl. The active fire area mean from scaled-FRP is close to the FLAMBE mean, and the Dual-Band active fire area is 7–10 times smaller than those.

3. Results

3.1. Evaluation of fire input configurations

Figure 2 presents the relationship between the plume-rise model injection heights and the MISR plume heights for the various fire input parameters (Table 2 and Table 3). For clarity, they are also shown for 500-m bins of MISR plume heights.

It is apparent that the plume model gives different injection heights depending on the input used, and we explore the sensitivity to key parameters below. Overall, the plume-rise model does not reproduce well the smoke heights observed by MISR as the maximum r^2 obtained is 0.33. The FLAMBE-Pxl/FRPx10 (Figure 2h) and scaled-FRP/FRPx10 (Figure 2p) show the best fit to the MISR observations. The WRF-Pxl/FT06 (Figure 2a) and WRF-Pxl/FUEL (Figure 2b) configurations give the largest injection heights, in particular for the lowest plumes observed by MISR. The overestimate for these configurations results from the combination of larger fire areas and total heat flux values used as inputs. The fire areas for WRF-Pxl are more than one order of magnitude larger than those of the other three approaches (Table 3). The FT06 and FUEL heat fluxes are on average twice as large as the FRPx10 and Dual-Band ones, for forest fires, which represent 35% of the plumes in the dataset. Based on these results, we discuss further the scaled-FRP/FRPx10 (Figure 2p) configuration; we consider it the best approach for estimating the fire areas and heat fluxes for use in the plume rise model, as it gives the best fit to the MISR observations (r^2=0.33). Additionally, we discuss further WRF-Pxl/FT06 since it has been adopted by the WRF-Chem model framework [*e.g. Pfister et al., 2011; Sessions et al., 2011]*.

To better interpret the model results relative to the fire inputs, we examine in more detail the model injection heights as a function of active fire area and total heat flux for four of the 16 configurations: WRF-Pxl/FT06, WRF-Pxl/FRPx10, scaled-FRP/FT06 and scaled-FRP/FRPx10, and compare them to the observed MISR heights (Figure 3). We also show the relationship between total heat flux and fire area for WRF-Pxl/FT06 and WRF-Pxl/FRPx10 in Figure 4.

As shown in Figure 3, MISR plume heights increase with fire area, regardless of the method used to estimate the active fire area, although significant variability is present in the distributions. The median height of large fires (i.e., > 850 ha in WRF-Pxl and > 150 ha in scaled-FRP) are 1.5–1.8 km higher than those of small fires (i.e., < 100 ha in WRF-Pxl and < 2.5 ha in scaled-FRP). This is consistent with the results of *Val Martin et al.* [2010], who showed that MISR plume heights were related to MODIS FRP with significant variability in a log-log relationship, and the fact that we use MODIS FRP and fire pixels as the basis for estimating fire area. Obviously, similar results are reflected in the model injection heights, as the model is sensitive to the fire area and heat flux values. For example, WRF-Pxl/FT06 (Figure 3a) provides the plume-rise model with large values of fire area and heat flux, and the medians of the simulated injection heights are typically at least 1 km higher than the observations. Conversely, scaled-FRP/FT06 initializes the model with lower fire areas than WRF-Pxl/FT06, and the simulated median injection heights are on an average 0.5 km lower than those simulated in WRF-Pxl/FT06, although still 0.5 km higher than the observations.

The WRF-Pxl/FRPx10 and scaled-FRP/FRPx10 configurations use lower heat flux values than WRF-Pxl/FT06 and scaled-FRP/FT06. In FRPx10 80% of the cases have heat flux values <10 kW/m^2, compared to only 6% in FT06. Figure 4 shows that for WRF-Pxl/FRPx10 a good linear correlation (r^2=0.7) exits between fire area and heat flux since both parameters are estimated using FRP values at each MODIS fire pixel. Hence, smaller fires (i.e., with fewer number of fire pixels and/or lower FRP values) tend to have lower fire energy emission rates. Similar relationships are found for scaled-FRP/FT06 and scaled-FRP/FRPx10 (not shown), with lower values for active fire areas and total heat fluxes (Table 3). In the case of WRF-Pxl/FT06 (and scaled-FRP/FT06), no relationship exists between fire area and heat flux, as only three values, which depend on vegetation type, are used for total heat flux, as described in section 2.4.1.

An important property of the plume-rise model is its ability to predict which plumes reach the FT. Figure 5 shows the relationship between injection height predicted by the model and observed by MISR, and highlights the plumes that are located in the FT, for the WRF-Pxl/FT06 and scaled-FRP/FRPx10 configurations. Following *Kahn et al.* [2008], we consider a smoke plume to be in the free troposphere with high confidence when the (plume-BL) height difference is > 500 m, to account for errors in both the MISR heights and the GEOS BL heights. We also report below results when the (plume-BL) height difference exceeds zero. The WRF-Pxl/FT06 case implies that 77–94% of the plumes reaching the FT (defined as (plume-BL) height>500 m and (plume-BL) height>0 m, respectively), whereas the fractions for the MISR data are 24–48%. As expected, the scaled-FRP/FRPx10 configuration implies a lower fraction of plumes in the FT, 16–35%, closer to the MISR results. However, the model does not put the correct plumes in the FT. As shown in Figure 5b, the MISR data implies that 137 plumes are in the FT, whereas the model puts only 75 plumes there, and only 42 plumes are in the FT according to both MISR and the model. In practice, the model locates 44% (33 out of 137) of the plumes in the FT and misses 70% (95 out 137) of the MISR plumes in the BL

3.2. Effect of atmospheric stability on simulated injection height

Val Martin et al. [2010] demonstrated the important effect of the atmospheric structure on the ultimate rise of fire emissions, as proposed by *Kahn et al.* [2007]. We illustrate the model sensitivity to the heat flux and fire area for two very different cases of atmospheric stability for the two representative plumes shown in Figure 1. We consider atmospheric stability as the change in potential temperature with height [*Holton*, 1992] at the location and time of the MISR plumes, as in the work of *Kahn et al.* [2007] and *Val Martin et al.* [2010]. Figure 6 depicts the atmospheric conditions for the two MISR plumes used as examples, and the results of the final injection heights as a function of the active fire area and total heat flux. We show model results for total heat flux ranging from 1 to 100 kW/m^2 and active fire area ranging from 1 to 250 ha, which are the range of values obtained with the scaled-FRP/FRPx10 approach.

The profile in Figure 6a shows the existence of a weak, broad stable layer, with maximum of 5 K/km centered at about 3 km altitude and 3 km deep, whereas the profile in Figure 6c shows a strong stable layer, with maximum of 16 K/Km, centered at 750 m and 1 km deep. These two cases exhibit similar wind speed conditions (not shown). For the "strong stability" case (Figures 6c,d), the model simulates a plume height that varies from 0.5 to 2.4 km over the range of input studied; for the "weak stability" case (Figures 6a,b), the range is from 0.6 to 4.3 km. The model gives different injection heights due to the presence of the strong, low altitude stable layer in the "strong stability" case that causes the simulated plume to lose vertical velocity faster than in the "weak stability" case, as explained by *Freitas et al.* [2007] in a sensitivity test performed with two different thermodynamic conditions. In that work, *Freitas et al.* [2007] also highlighted the weak sensitivity of the model to the heat flux values. We find, however, that the model also has a low sensitivity to fire area because a given plume height is associated with multiple combinations of these two input parameters. For example, in the "weak stability" case, a plume height of 3 km can be obtained with model simulations that use fire area ranging from 25 to 150 ha, and total heat flux from 25 to 100 kW/m^2.

Based on a simple 1-D convective parcel model, *Kahn et al.* [2007] showed that, in addition to atmospheric stability structure and total heat flux, entrainment is a complex parameter associated with atmospheric stability that can affect significantly the final rise of the plume. As described in *Freitas et al.* [2010] and mentioned in section 2.2, two entrainment parameters are included in the plume rise model: lateral entrainment, to account for the loss of buoyancy due to entrainment of cold air into the plume; and dynamic entrainment, to account for the horizontal displacement of the plume due to wind drag. Both parameters are inversely proportional to the plume radius. In the plume-rise model, the formulation for the lateral entrainment coefficient is $2\alpha R^{-1}$, in which R is the radius of the plume and α is assumed equal to 0.05 [*Freitas et al.*, 2010]. We tested slightly smaller and larger entrainment coefficients (i.e., α of 0.025 and 0.1) using the scaled-FRP/FRPx10 configuration. The mean injection heights were 14% larger with α equal to 0.025 and 12% smaller with α equal to 0.1. However, the change in entrainment coefficients did not significantly improve the correlation between the model injection heights and the observed MISR plume heights (that is, the r^2 was about 0.3).

3.3. Constraints for smoke plume rise

As shown in section 3.1, constraining quantitatively the plume-rise model with observations is a difficult task due to the uncertainty in the input parameters. Clearly, some previous assumptions adopted in 3-D models do not match the MISR plume heights at all well. Here we propose a simplified approach for computing plume injection heights using two main physical factors: buoyancy flux and atmospheric stability structure. This analysis is based on the findings presented in *Val Martin et al.* [2010] for the entire MISR dataset. The authors showed that plumes reaching the FT have larger FRP values that those trapped within the BL, and that the depth of the BL and the presence of stable layer in the FT influence the smoke plume height. To illustrate our simple approach, we classified the MISR plumes by altitude and analyzed the atmospheric stability structure and fire radiative conditions within this classification. Figure 7 displays the results for three cases: observations of low-altitude (<1000 m), medium-altitude (1000-2500 m) and high-altitude (>2500 m) plumes, and Table 4 summarizes the statistics of the parameters in these categories for all observations and by biome type. This analysis shows that smoke plumes reaching high altitudes exhibit statistically higher FRP than those at low altitude, with a mean of about 2100 MW higher. In addition, plumes reaching high altitudes are associated with weaker atmospheric stability conditions, and plumes with low altitude get confined below the BL, consistent with *Val Martin et al.* [2010]. For example, the atmospheric stability of high plumes (Figure 7f) is most often lower than 10 K/Km, whereas it frequently reaches more than 10 K/km in low-altitude plumes (Figure 7b). In addition, a distinct stable layer at around 1500 m is typically present in low plumes, and smoke never punches through this layer, which represents the BL cap. In contrast, a distinct layer, if present, appears at about 2000-2500 m in high plumes, and smoke often punches through. Results from medium-altitude plumes (Figure 7d) show intermediate behavior. We replicated these analyses stratified by biome, and found similar patterns, with different FRP values, representative of forest and shrubland fires (large FRP) and grassland fires (small FRP). However, further subdivision of the data reduced the sample sizes, and some results were not statistically robust, in particular for grassland fires (Table 4).

In Figure 8, we classify the observations further by atmospheric stability and plume height, to investigate the fire radiative heat under these conditions. We consider highly stable those atmospheric profiles having stable layers with stability above 10 K/km (e.g, Figure 6c), weakly stable those atmospheres with stability below 10 K/km (e.g., Figure 6a), and neutrally stable those without a distinct stable layer. Figure 8 shows that high FRP values are associated with stronger atmospheric stability in each plume elevation category. Fires with low altitude smoke are associated with larger FRP values in highly stable conditions (246 MW) than in weakly stable (164 MW) and neutrally stable (136 MW) ones. A similar pattern is found for fires with smoke that reaches altitudes of 1000–2500 m (867, 412 and 316 MW, respectively). We have fewer observations for fires with high altitude smoke, so the distributions are not statistically representative. However, it is clear in Figure 8 that the more stable the atmosphere, the larger the FRP associated with a given height category, suggesting greater buoyancy flux is required for the smoke to reach similar altitudes, as expected on physical grounds.

4. Discussion and Conclusions

We used MISR plume heights over North America to evaluate the ability of the plume-rise model described in Freitas et al., (2007,2010) to produce accurate injection heights. We initialized the model with GEOS assimilated meteorological fields and estimated fuel moisture content at the locations and times of the MISR observations. We tested the model

with four estimates each for active fire area and total sensible heat flux. The analysis shows that the plume-rise model gives different injection heights depending on the input used, and is not able to reproduce the plume heights observed by MISR uniformly, over the range of conditions studied (maximum r^2 is 0.33 in Figure 2). In addition, the model fails to locate the right plumes above the BL (Figure 5), although this is crucial information needed for atmospheric models to simulate properly the dispersion of fire emissions.

Val Martin et al. [2010] analyzed a 5-year record of MISR plume heights over North America (3367 plumes) using different definitions of plume heights. Our analysis showed that, using the best estimated median of the vertical distribution of stereo-height retrievals for the entire plume, 4–12% of the plumes reach the FT (*i.e.*, plume-BL height>500 m), depending on the year. These fractions were higher, 15–28%, for the best estimated maximum plume height of the distribution. Using a less conservative definition for a plume residing in the FT (*i.e.*, plume-BL height>0 m), the fractions were 17–30% and 38–55% for the best estimated median and maximum height, respectively. Here, we modified our previous definition of plume height to be compatible to the injection height simulated by the plume-rise model, and considered the best estimated maximum height above the fire source. Using this plume height definition and a smaller number of observations (584 plumes), we find that 24–48% of the plumes reach the FT (defined as (plume-PBL) height>500 m and (plume-PBL) height>0 m, respectively). It is important to note that the maximum plume height definition does not imply that the entire plume is above the BL, as plumes are typically about 850 m thick and some fraction of the smoke may remain in the BL [*Val Martin et al.*, 2010].

Our plume-rise model simulations using the scaled-FRP/FRPx10 configuration show that these input settings initially provided the best fit to the observed MISR plume heights, since they give a fraction of plumes in the FT closest to that observed by MISR (16-35% versus 24-48%). However, a more detailed analysis (Figure 5b) indicates that the model incorrectly locates 44% of the plumes in the FT, whereas it misses 70% of the actual cases where the plume is in the FT.

Brioude et al. [2009] used the plume-rise module with the FLEXPART Lagrangian Particle Dispersion Model to study the impact of biomass burning on clouds off the California coast. In that work, the fire size and heat flux for each fire were retrieved from WF-ABBA; for the heat flux, they used our approach, which assumes that radiant energy is approximately 10% of the total heat energy released by the fire. Using these fire settings, and comparing the injection heights to the FLEXPART BL, they reported that 30% of the plumes reach the FT. However, they did not have observations to evaluate the modeled injection heights.

The current configuration in the WRF-Chem plume-rise module (*i.e.*, WRF-Pxl/FT06) does not give the model the correct fire inputs. The model overestimates the injection height significantly, and locates 77–94% of the plumes in the FT (Figure 5a), as determined by the GEOS BL heights. This setting uses only five heat flux values taken from conditions appropriate for Brazil and applies them to fires in North America. *Sessions et al.* [2011] compared injection heights simulated by WRF-Chem with an embedded plume-rise model to MISR heights obtained during the ARCTAS campaign over Siberia and Canada in 2008. They used two preprocessing configurations to determine fire locations and fire size: one is the default in WRF-Chem and relies on WF-ABBA and MODIS pixels, the other is based on the FLAMBE dataset. In a 10-day run, the WRF-Chem placed more than 75% of the plumes above the BL, for both configurations. Similarly, *Pfister et al.* [2011] reported that the WRF-Chem plume-rise module released about 50% of the emissions into the FT in a study over California during ARCTAS-CARB. Using the same definition for plumes above the BL (i.e., [plume height-BL]>0 km), our analysis indicates that a larger fraction of plumes reaches the FT (94%). As discussed in detail by *Sessions et al.* [2011], WRF-Chem BL heights are lower than GEOS BL heights due to different BL schemes. In addition, analysis of plumes from different locations, different plume model versions (with and without wind effects) and different meteorological fields may be also responsible for the differences in our results regarding the fractions above the BL. In any case, it is clear that the plume-rise module package supported by WRF-Chem overestimates the injection height compared with MISR observations, that indicate typically about 24–48% of plumes reach the FT over North America.

Based on previous studies [*e.g. Kahn et al., 2007; Freitas et al., 2007*], it is clear that smoke plume rise is governed by buoyant energy produced by the fire, ambient atmospheric stability and entrainment. In addition, latent heat release and wind are additional factors that can affect plume rise [*Freitas et al.*, 2010]. However, our analyses show that constraining the plume-rise model quantitatively is a difficult task, due to uncertainty in the input parameters. Since the buoyant energy varies significantly depending on the fire type, and typically exhibits strong heterogeneity across active burning areas, it is difficult to measure directly. The model assumes that sensible heat flux is 55% of the total heat flux, and we further infer total heat flux from instantaneous fire radiative measurements made by MODIS, considering that 10% of the total heat flux is radiant energy. However, MODIS FRP measurements may be uncertain for several reasons. For example, the presence of dense smoke can lead to underestimates of the FRP, and the relationship between observed spectral signals and FRP can depend on the spectral emissivity assumed in the retrieval, which likely varies depending upon the fire dynamics (e.g., smoldering versus flaming) and flame thickness. [*Kahn et al.*, 2007].

The atmospheric conditions used to constrain the plume-rise model are often obtained from global or regional atmosphere models, and the coarse spatial and temporal resolution can introduce uncertainties in the atmospheric stability calculation and the boundary layer heights [*Val Martin et al.*, 2010; *Sessions et al.*, 2011]. Entrainment is a yet more difficult parameter to constrain given current knowledge, as it depends on small-scale interactions between the plume and the surrounding environment [*Kahn et al.*, 2007]. In the plume-rise model, lateral and dynamic entrainment are parameterized with simple coefficients inversely proportional to the cross-sectional basal area of the plume, which is taken from the active fire area estimate. However, fires typically have non-circular cross-sections, and burning generally does not occur at a uniform temperature.

Other challenges in modeling fire emissions are the diurnal and seasonal fire intensity variations, which are not taken into account by the plume-rise module used in this study, as it relies uniquely on five heat flux values depending only on vegetation type. Evaluation of the plume-rise model is limited in our case to the MISR observation time, which are 11:00-13:45 local time for our dataset [*Val Martin et al.*, 2010]. The MISR local observing time does not coincide with the maximum in fire intensity, which typically occurs in the afternoon [*e.g. Giglio et al., 2006; Vermote et al., 2009; Mu et al., 2011*]. The MODIS FRP diurnal cycle indicates that fire intensity peaks between 13:00 to 17:00 in a variety of biomes [*Giglio*, 2007; *Roberts et al.*, 2009; *Vermote et al.*, 2009]. Furthermore, *Val Martin et al.* [2010] compared the variability of MISR plume heights and MODIS FRP on a monthly basis, and concluded that the annual variability of plume heights was driven mainly by the annual cycle of fire radiative heat.

The use of a plume-rise model requires the calculation of an injection height for each fire, obtained by numerical integration of a system of equations. This numerical approach makes the process computationally expensive [*Freitas et al.*, 2007; *Guan et al.*, 2008]. In addition, the validation of the plume-rise model has been based to date on a few case studies, with the exception of the work of *Sessions et al.* [2011]. Here, using a large plume dataset and several approaches to estimate fire properties, we demonstrate that the model currently does not simulate properly the plume heights, and this implies that embedding the plume-rise model using the currently available fire constraints in large-scale atmospheric models is not a realistic approach.

Our analysis of the main physical constraints for smoke plume rise (Figures 7 and 8, and Table 4) shows that smoke plumes reaching high altitudes exhibit higher FRP and weaker atmospheric stability conditions than those at low altitude, which tend to be confined below the BL. The simplified relationship of FRP and atmospheric stability, summarized in Table 4, can be used as a basis to develop an inexpensive, empirically based parameterization for computing the plume injection heights for fires. It is important to note that entrainment is also a key factor that drives plume rise, but we could not constrain it with the information available to date.

A number of FRP-based emission inventories have been developed recently, *e.g.*, the Global Fire Assimilation System (GFAS) [*Kaiser et al.*, 2012] and the Quick Fire Emission Dataset (QFED) [da Silva, NASA, personal communication], and successfully incorporated into CTMs. For example, QFED is operational in the GEOS-5 aerosol forecasting system and Goddard Chemistry Aerosol Radiation and Transport (GOCART) model [*Petrenko et al.*, 2012], whereas GFAS is used within the operational forecasting system being developed for European monitoring of the global atmosphere (http://www.gmes-atmosphere.eu/). Most commonly, however, CTMs use biomass burning emission inventories derived from satellite measurements of post-fire burned area and estimates of biomass consumed per unit area, *e.g.*, the Global Fire Emissions Database (GFED) [*van der Werf et al.*, 2010]. A number of studies have shown a direct linear relationship between FRP and biomass consumed [*e.g. Wooster et al., 2005; Freeborn et al., 2008]*, and a set of empirically derived factors have been developed to relate satellite-derived FRP to combustion rates from different biomes [*e.g. Kaiser et al., 2012]*. These factors may be used inversely to connect the fuel consumption values reported in the GFED inventory to FRP values, on a monthly or daily basis. Thus, CTMs could use the information on atmospheric stability and FRP or a direct relationship to FRP to treat empirically the injection heights on large-scale studies.

Another simplified parameterization yet to be tested is based on the statistical analysis of MISR plume climatologies for extratropical [*Val Martin et al.*, 2010] and tropical [*Tosca et al.*, 2011] biomes. Based on the MISR observations, we recommend injecting about 15% of the emissions into the FT for extra-tropical forest and shrubland fires and about 5% for tropical forest and grassland fires. Fire emissions released in the BL will be mixed throughout the BL, whereas emissions released in the FT will be injected at the height of the stable layer or spread-out vertically in those model vertical grid boxes without distinct atmospheric stable layers, following the work of *Val Martin et al.* [2010].

To reduce the uncertainty associated with plume rise models, we recommend small-scale, simultaneous field measurements of all the parameters driving smoke plume-rise. The necessity of new field campaigns to quantitatively characterize plume rise has also been recommended by *Ichoku et al.* [2012] after a comprehensive review of satellite observations on biomass burning for atmospheric modeling. In future work, we will explore the implementation of the simplified injection height parameterizations within a CTM.

Appendix A: Development of a fuel consumption map over the North America boreal region

Previous studies have shown that current estimates for fuel consumption in boreal forest fires are underestimated [*e.g. Amiro et al., 2001; Kasischke and Bruhwiller, 2002; Turquety et al., 2007]*. We developed a new map of fuel consumption using the U.S. Forest Service (USFS) CONSUME model (version 3) [*Ottmar*, 2009], adapted for boreal ecosystems. This model uses as input fuel loading and moisture conditions, and produces estimates of fuel consumption. It is designed to use the fuel loadings for the Fuel Characteristic Classification System (FCCS) for the U.S. (lower 48 states and Alaska) [*Ottmar and Baker*, 2007]. CONSUME requires maps of fuelbeds. For Canada, fuelbed information at 1-km resolution was obtained from the Canadian Fire Behavior Prediction (FBP) system, which is based on satellite-derived vegetation data [*Nadeau et al.*, 2005]. For Alaska, we used a map created by the USFS, which follows the classification scheme of *Nadeau et al.* [2005] [Martin Parker, USFS, personal communication]. We mapped the Canadian fuelbeds onto their corresponding type in the U.S. FCCS [*Ottmar and Baker*, 2007]. Some assumptions were needed to match some of the Canadian FBP fuelbed types into the U.S. FCCS classification system [Nancy French, MTRI, personal communication], and we summarize those in Table 5.

To compute fuel consumption, we then imported the FCCS fuel loading values for each fuelbed type into CONSUME. The effect of burning duff layer was considered within the fuel consumption values in the fuelbed, as CONSUME takes into account burning of the organic soil layer. We adjusted the organic soil layer in some of the fuelbed types for that purpose. For example, we increased the duff layer depth for Black spruce-feathermoss (FCCS 87) in CONSUME from 15 cm to 30 cm to match the description of deep, compacted organic layer from the Canadian FBP system (FBP C2).

To represent the changes in fuel moisture regime throughout the fire burning season, we computed fuel consumption values in each fuelbed type for five different types of moisture conditions (*i.e.*, wet, moist, moderately-dry, dry and extra-dry) and considered changes in moisture conditions in the three fuelbed stratum given in CONSUME (*i.e.*, woody fuels of 0.6-3 cm diameter (10-hr), woody fuels of 8-20 cm diameter (1000-hr) and duff). Table 6 summarizes the fuel moisture percentages for the fuelbed stratum in each moisture category. These fuel moisture conditions are based on typical conditions used in CONSUME and the Fire Emission Production Simulator (http://www.fs.fed.us/pnw/fera/feps/index.shtml); values are consistent with previous reports of soil moisture content, based on field measurements over the boreal region [*Ottmar and Baker*, 2007; *Jandt et al.*, 2005].

We derived fuel consumption maps at 1° latitude by 1° longitude for the five fuel moisture conditions, for use in climate and atmospheric models. Figure 9 shows the boreal region fuel consumption map for moderately-dry conditions as an example. We also include in the map the fuel consumption values for the lower 48 states described in *Spracklen et al.* [2009]. Table 3 summarizes the fuel consumption values for the fuelbed types by moisture conditions. In this work, to determine the total heat flux values (in W/m^2), we use the fuel consumption values obtained for moderately-dry conditions (Figure 9) and a standard heat of combustion for extra-tropical vegetation of 18.7e6 J/Kg [*Trentmann et al.*, 2006], and assuming that the average burning time of the fire is two hours.

Acknowledgments. This work was supported by grants from the National Science Foundation (ATM0554804) and NASA (NNX09AC51G) to Harvard University (MVM and JAL). The work of R. Kahn is supported in part by NASA's Climate and Radiation Research and Analysis Program under H. Maring, NASA's Atmospheric Composition Program under R. Eckman, and the NASA Earth Observing System MISR instrument project. We thank Saulo Freitas for providing and helping implement the 1D plume-rise model, Nancy French for helpful discussions about North American fuelbeds, Alan Cantin for access to the surface observations over Canada used to run FWI and Martin Parker for providing the Alaska fuelbed map. The work of David Nelson on the MISR plume climatology is gratefully acknowledged.

References

Achtemeier, G. L., S. A. Goodrick, Y. Liu, F. Garcia-Menendez, Y. Hu, and M. T. Odman (2011), Modeling smoke plume-rise and dispersion from southern united states prescribed burns with daysmoke, *Atmosphere*, *2*, 358–388, doi:10.3390/atmos2030358.

Amiro, B. D., J. B. Todd, B. M. Wotton, K. A. Logan, M. D. Flannigan, B. J. Stocks, J. A. Mason, D. L. Martell, and K. G. Hirsch (2001), Direct carbon emissions from canadian forest fires, 1959 to 1999, *Can. J. For. Res.*, *31*, 512–525.

Ayers, G. (2001), Comment on regression analysis of air quality data, *Atmos. Environ.*, *35*, 2423–2425.

Briggs, G. (1969), Plume rise, *Tech. Rep. Critical Review Series, TID-25075, National Technical Information Service, Springfield, VA, 81 pp*, USAEC.

Brioude, J., et al. (2009), Effect of biomass burning on marine stratocumulus clouds off the california coast, *Atmospheric Chemistry and Physics*, *9*(22), 8841–8856, doi:10.5194/acp-9-8841-2009.

Chatfield, R. B., and A. C. Delany (1990), Convection links biomass burning to increased tropical ozone: However, models will tend to overpredict o3, *J. Geophys. Res.*, *95*, 18,47318,488, doi:10.1029/JD095iD11.

Chen, Y., Q. Li, J. T. Randerson, E. A. L. R. A. Kahn, D. L. Nelson, and D. J. Diner (2009), The sensitivity of CO and aerosol transport to the temporal and vertical distribution of North American boreal fire emissions, *Atmos. Chem. Phys.*, *9*, 6559–6580.

Colarco, P. R., M. R. Schoeberl, B. G. Doddridge, L. T. Marufu, O. Torres, and E. J. Welton (2004), Transport of smoke from Canadian forest fires to the surface near Washington, D.C.: Injection height, entrainment, and optical properties, *J. Geophys. Res.*, *109*, D06203, doi:10.1029/2003JD004248.

Damoah, R., et al. (2006), A case study of pyro-convection using transport model and remote sensing data, *atmospheric chemistry and physics*, *6*, 173–185.

de Gouw, J. A., et al. (2006), Volatile organic compounds composition of merged and aged forest fire plumes from Alaska and western Canada, *J. Geophysic. Res.*, *111*, D10303, doi:10.1029/2005JD006175.

Dirksen, R. J., K. F. Boersma, A. T. J. de Laat, P. Stammes, G. R. van der Werf, M. Val Martin, , and H. M. Kelder (2009), An aerosol boomerang: rapid around-the-world transport of smoke from the December 2006 Australian forest fires observed from space, *J. Geophys. Res.*, *114*, D21201, doi:10.1029/2009JD012360.

Dozier, J. (1981), A method for satellite identification of surface temperature fields of subpixel resolution, *Remote Sensing of Environment*, *11*, 2212291, doi:10.1016/0034-4257(81)90021-3.

Freeborn, P., M. Wooster, W. Hao, C. Ryan, B. Nordgren, S. Baker, and C. Ichoku (2008), Relationships between energy release, fuel mass loss, and trace gas and aerosol emissions during laboratory biomass fires, *Journal of Geophysical Research*, *113*, D01102, doi:10.1029/2007JD008489.

Freitas, S. R., K. M. Longo, and M. O. Andreae (2006), Impact of including the plume rise of vegetation fires in numerical simulations of associated atmospheric pollutants, *Geophys. Res. Lett.*, *33*, L17808, doi:10.1029/2006GL026608.

Freitas, S. R., et al. (2007), Including the sub-grid scale plume rise of vegetation fires in low resolution atmospheric transport models, *Atmos. Chem. Phys.*, *7*, 3385–3398.

Freitas, S. R., K. M. Longo, J. Trentmann, and D. Latham (2010), Technical note: Sensitivity of 1-d smoke plume rise models to the inclusion of environmental wind drag, *Atmospheric Chemistry and Physics*, *10*(2), 585–594, doi:10.5194/acp-10-585-2010.

Fromm, M., R. Bevilacqua, R. Servranckx, J. Rosen, J. P. Thayer, J. Herman, and D. Larko (2005), Pyro-cumulonimbus injection of smoke to the stratosphere: Observations and impact of a super blowup in northwestern Canada on 3–4 August 1998, *J. Geophys. Res.*, *110*(D8), 1–16, doi:10.1029/2004JD005350.

Generoso, S., I. Bey, J.-L. Atti, and F.-M. Bron (2007), A satellite- and model-based assessment of the 2003 Russian fires: Impact on the Arctic region, *J. Geophys. Res.*, *112*, D15302, doi:10.1029/2006JD008344.

Giglio, L. (2007), Characterization of the tropical diurnal fire cycle using virs and modis observations, *Remote. Sens. Environ.*, *108*(4), 407–421.

Giglio, L., I. Csiszar, and C. O. Justice (2006), Global distribution and seasonality of active fires as observed with the Terra and Aqua Moderate Resolution Imaging Spectroradiometer (MODIS) sensors, *J. Geophys. Res.*, *111*, D02016, doi:10.1029/2005JG000142.

Grell, G., S. R. Freitas, M. Stuefer, and J. Fast (2011), Inclusion of biomass burning in wrf-chem: impact of wildfires on weather forecasts, *Atmospheric Chemistry and Physics*, *11*(11), 5289–5303, doi:10.5194/acp-11-5289-2011.

Guan, H., R. B. Chatfield, S. R. Freitas, R. W. Bergstrom, and K. M. Longo (2008), Modeling the effect of plume-rise on the transport of carbon monoxide over Africa with NCAR CAM, *Atmos. Chem. Phys.*, *8*, 6801–6812.

Guan, H., R. Esswein, J. Lopez, R. Bergstrom, A. Warnock, M. Follette-Cook, M. Fromm, and L. T. Iraci (2010), A multi-decadal history of biomass burning plume heights identified using aerosol index measurements, *Atmospheric Chemistry and Physics*, *10*(14), 6461–6469, doi:10.5194/acp-10-6461-2010.

Holton, J. R. (1992), *An Introduction to Dynamic Meteorology*, Elsevier New York.

Hyer, E. J., and J. S. Reid (2009), Baseline uncertainties in biomass burning emission models resulting from spatial error in satellite active fire location data, *Geophys. Res. Lett.*, *36*, L05802, doi:10.1029/2008GL036767.

Hyer, E. J., D. J. Allen, and E. S. Kasischke (2007), Examining injection properties of boreal forest fires using surface and satellite measurements of CO transport, *J. Geophys. Res.*, *112*, D18307, doi:10.1029/2006JD008232.

Ichoku, C., R. Kahn, and M. Chin (2012), Satellite contributions to the quantitative characterization of biomass burning for climate modeling, *Atmos. Res.*, doi:10.1016/j.atmosres.2012.03.007.

Jandt, R., A. J., and H. E. (2005), Forest floor moisture content and fire danger indices in alaska, *Tech. rep.*, Department of the Interior, Bureau of Land Management BLM/AK/ST-05/009+9218+313, Alaska Technical Report 54.

Kahn, R. A., W.-H. Li, C. Moroney, D. J. Diner, J. V. Martonchik, and E. Fishbein (2007), Aerosol source plume physical characteristics from space-based multi-angle imaging, *J. Geophys. Res.*, *112*, D11205, doi:10.1029/2006JD007647.

Kahn, R. A., Y. Chen, D. L. Nelson, F.-Y. Leung, Q. Li, D. J. Diner, and J. A. Logan (2008), Wildfire smoke injection heights - Two perspectives from space, *Geophys. Res. Lett.*, *35*, L04809, doi:10.1029/2007GL032165.

Kaiser, J. W., et al. (2012), Biomass burning emissions estimated with a global fire assimilation system based on observed fire radiative power, *Biogeosciences*, *9*, 527554.

Kasischke, E. S., and L. P. Bruhwiller (2002), Emissions of carbon dioxide, carbon monoxide, and methane from boreal forest fires in 1998, *J. Geophys. Res.*, *108*, doi:10.1029/2001JD000461.

Labonne, M., F.-M. Breon, and F. Chevallier (2007), Injection height of biomass burning aerosols as seen from a spaceborne lidar, *Geophys. Res. Lett.*, *34*, L11806, doi:10.1029/2007GL029311.

Lamarque, J.-F., et al. (2003), Identification of co plumes from MOPITT data: Application to the August 2000 Idaho-Montana forest fires, *Geophys. Res. Lett.*, *30 (13)*, 1688, doi:10.1029/2003GL017503.

Latham, D. (1994), PLUMP: A one-dimensional plume predictor and cloud model for fire and smoke managers, *Tech. Rep. General Technical Report INT-GTR-314*, Intermountain Research Station, USDA Forest Service.

Lavoue, D., C. Liousse, H. Cachier, B. J. Stocks, and J. G. Goldammer (2000), Modeling of carbonaceous particles emitted by boreal and temperate wildfires at northern latitudes, *J. Geophys. Res.*, *1035*(D22), 26,87126,890.

Leung, F.-Y. T., J. A. Logan, R. Park, E. Hyer, E. Kasischke, D. Streets, and L. Yurganov (2007), Impacts of enhanced biomass burning in the boreal forests in 1998 on tropospheric chemistry and the sensitivity of model results to the injection height of emissions, *J. Geophys. Res.*, *112*(D10), D10313, doi:10.1029/2006JD008132.

Liu, Y., G. L. Achtemeier, S. Goodrick, and W. A. Jackson (2010), Important parameters for smoke plume rise simulation with daysmoke, *Atmospheric Pollution Research*, *1*, 250259.

Lucchesi, R. (2007), File specification for GEOS-5 DAS gridded output global modeling and assimilation office version 6.3, Goddard Space Flight Center, Greenbelt, Maryland. Published on the web, http://gmao.gsfc.nasa.gov/operations/GEOS5_V1_File_Specification.pdf.

Mims, S. R., R. A. Kahn, C. M. Moroney, B. J. Gaitley, D. L. Nelson, and M. J. Garay (2010), MISR stereo-heights of grassland fire smoke plumes in Australia, *IEEE Trans. Geosci. Remote Sens.*, *48*, 25–35, doi:10.1109/TGRS.2009.2027114.

Mu, M., et al. (2011), Daily and 3-hourly variability in global fire emissions and consequences for atmospheric model predictions of carbon monoxide, *J. Geophys. Res.*, *116*, D24303, doi:10.1029/2011JD016245.

Nadeau, L., D. McRae, and J.-Z. Jin (2005), Development of a national fuel-type map for canada using fuzzy logic, *Tech. rep.*, Nat. Resour. Can., Edmonton, AB. Inf. Rep. NOR-X-406.

Nelson, D., C. Averill, S. Boland, R. Morford, M. Garay, C. Thompson, J. Hall, D. Diner, and H. Camphell (2008a), MISR Interactive eXplorer (MINX) v1.0 User's Guide, Jet Propulsion Lab, NASA. Published on the web, https://www.openchannelsoftware.com/projects/MINX.

Nelson, D., C. Lawshe, D. Mazzoni, D. Diner, and R. Kahn (2008b), MISR plume height climatology project: Quality statement and error and bias analysis, Jet Propulsion Lab, NASA. Published on the web, http://www-misr2.jpl.nasa.gov/EPA-Plumes/suggestions4UsingData.cfm.

Ottmar, R., and S. Baker (2007), Forest floor consumption and smoke characterization in boreal forested fuelbed types of alaska, *Tech. Rep. Final Report, JFSP Project Number 03-1-3-08*, US Forest Service.

Ottmar, R. D. (2009), Consume 3.0–a software tool for computing fuel consumption, *Tech. Rep. Fire Science Brief. Issue 55, Page 1-6, JFSP Project Number 98-1-9-06*, US Forest Service.

Petrenko, M., R. Kahn, M. Chin, A. Soja, T. Kucsera, and Harshvardhan (2012), The use of satellite measured aerosol optical depth to constrain biomass burning emissions source strength in a global model gocart, *J. Geophys. Res.*, *in review*.

Pfister, G. G., et al. (2006), Ozone production from the 2004 North American boreal fires, *J. Geophys. Res.*, *111*(D24), D24S07, doi:10.1029/2006JD007695.

Pfister, G. G., J. Avise, C. Wiedinmyer, D. P. Edwards, L. K. Emmons, G. D. Diskin, J. Podolske, and A. Wisthaler (2011), Co source contribution analysis for california during arctas-carb, *Atmospheric Chemistry and Physics*, *11*(15), 7515–7532, doi:10.5194/acp-11-7515-2011.

Raffuse, S. M., K. J. Craig, N. K. Larkin, T. T. Strand, D. C. Sullivan, N. J. M. Wheeler, and R. Solomon (2012), An evaluation of modeled plume injection height with satellite-derived observed plume height, *Atmosphere*, *3*(1), 103–123, doi:10.3390/atmos3010103.

Reid, J., et al. (2009), Global monitoring and forecasting of biomass-burning smoke: Description and lessons from the fire locating and modeling of burning emissions (flambe) program, *IEEE Journal of Special Topics in Applied Earth Observations and Remote Sensing*, *2*, 144–162.

Rio, C., F. Hourdin, and A. Chédin (2010), Numerical simulation of tropospheric injection of biomass burning products by pyrothermal plumes, *Atmospheric Chemistry and Physics*, *10*(8), 3463–3478, doi:10.5194/acp-10-3463-2010.

Roberts, G., M. Wooster, and E. Lagoudakis (2009), Annual and diurnal african biomass burning temporal dynamics, *Biogeosciences*, *6*, 849–866.

Schroeder, W., I. Csiszar, L. Giglio, and C. C. Schmidt (2010), On the use of fire radiative power, area, and temperature estimates to characterize biomass burning via moderate to coarse spatial resolution remote sensing data in the brazilian amazon, *J. Geophys. Res.*, *115*, D21121, doi:10.1029/2009JD013769.

Sessions, W. R., H. E. Fuelberg, R. A. Kahn, and D. M. Winker (2011), An investigation of methods for injecting emissions from boreal wildfires using wrf-chem during arctas, *Atmospheric Chemistry and Physics*, *11*(12), 5719–5744, doi:10.5194/acp-11-5719-2011.

Sofiev, M., T. Ermakova, and R. Vankevich (2012), Evaluation of the smoke-injection height from wild-land fires using remote-sensing data, *Atmospheric Chemistry and Physics*, *12*(4), 1995–2006, doi:10.5194/acp-12-1995-2012.

Spracklen, D. V., J. A. Logan, L. J. Mickley, R. J. Park, R. Yevich, A. L. Westerling, and D. A. Jaffe (2007), Wildfires drive interannual variability of organic carbon aerosol in the western u.s. in summer, *Geophys. Res. Lett.*, *34*, L16816, doi:10.1029/2007GL030037.

Spracklen, D. V., L. J. Mickley, J. A. Logan., R. C. Hudman, R. Yevich, M. D. Flannigan, and A. L. Westerling (2009), Impacts of climate change from 2000 to 2050 on wildfire activity and carbonaceous aerosol concentrations in the western United States, *J. Geophys. Res.*, *114*, D2030, doi:10.1029/2008JD010966.

Stein, A. F., G. D. Rolph, R. R. Draxler, B. Stunder, and M.Ruminsk (2009), Verification of the noaa smoke forecasting system: Model sensitivity to the injection height, *Wea. Forecasting*, *24*, 379–394, doi:http://dx.doi.org/10.1175/2008WAF2222166.1.

Tosca, M., J. Randerson, C. Zender, D. Nelson, D. Diner, and J. Logan (2011), Dynamics of fire plumes and smoke clouds associated with peat and deforestation fires in indonesia, *Journal of Geophysical Research*, *116*, D08207, doi:10.1029/2010JD015148.

Trentmann, J., M. O. Andreae, H.-F. Graf, P. V. Hobbs, R. D. Ottmar, and T. Trautmann (2002), Simulation of a biomass-burning plume: Comparison of model results with observations, *J. Geophys. Res.*, *107*, D24013, doi:10.1029/2001JD000410.

Trentmann, J., G. Luderer, T. Winterrath, M. Fromm, R. Servranckx, C. Textor, M. Herzog, H.-F. Graf, and M. O. Andreae (2006), Modeling of biomass smoke injection into the lower stratosphere by a large forest fire (part I): Reference simulation:, *Atmos. Chem. Phys.*, *6*, 5247–5260.

Turquety, S., et al. (2007), Inventory of boreal fire emissions for North America in 2004: Importance of peat burning and pyroconvective injection, *J. Geophys. Res.*, *112*(D12), D12S03, doi:10.1029/2006JD007281.

Val Martin, M., R. Honrath, R. C. Owen, G. Pfister, P. Fialho, and F. Barata (2006), Significant enhancements of nitrogen oxides, ozone and aerosol black carbon in the North Atlantic lower free troposphere resulting from North American boreal wildfires, *J. Geophys. Res.*, *111*, D23S60, doi:10.1029/2006JD007530.

Val Martin, M., J. A. Logan, R. A. Kahn, F.-Y. Leung, D. L. Nelson, and D. J. Diner (2010), Smoke injection heights from fires in north america: analysis of 5 years of satellite observations, *Atmospheric Chemistry and Physics*, *10*(4), 1491–1510, doi:10.5194/acp-10-1491-2010.

van der Werf, G. R., et al. (2010), Global fire emissions and the contribution of deforestation, savanna, forest, agricultural, and peat fires (19972009), *Atmospheric Chemistry and Physics*, *10*(23), 11,707–11,735, doi:10.5194/acp-10-11707-2010.

Van Wagner, C. E. (1987), Development and structure of the Canadian forest fire, weather index system, *Tech. Rep. Forestry Technical Report 35, 37 p.*, Canadian Forest Service.

Vermote, E., E. Ellicott, O. Dubovik, T. Lapyonok, M. Chin, L. Giglio, and G. J. Roberts (2009), An approach to estimate global biomass burning emissions of organic and black carbon from modis fire radiative power, *J. Geophys. Res.*, *114*, D18205, doi:10.1029/2008JD011188.

Wang, J., S. A. Christopher, U. S. Nair, J. S. Reid, E. M. Prins, J. Szykman, and J. L. Hand (2006), Mesoscale modeling of central american smoke transport to the united states: 1. top-down assessment of emission strength and diurnal variation impacts, *J. Geophys. Res.*, *111*, D05S17, doi:10.1029/2005JD006416.

Wofsy, S. C., et al. (1992), Atmospheric chemistry in the arctic and subarctic: Influence of natural fires, industrial emissions, and stratospheric inputs, *J. Geophys. Res.*, *97*, 116,73116,746, doi:10.1029/92JD00622.

Wooster, M., B. Zhukov, and D. Oertel (2003), Fire radiative energy for quantitative study of biomass burning: derivation from the bird experimental satellite and comparison to modis fire products, *Remote Sensing of Environment*, *86*, 83107.

Wooster, M., G. Roberts, G. Perry, and Y. Kaufman (2005), Retrieval of biomass combustion rates and totals from fire radiative power observations: calibration relationships between biomass consumption and fire radiative energy release, *Journal of Geophysical Research*, *110*, D21111, doi: 10.1029/2005JD006318.

Wooster, M., W. Xu, and T. Nightingale (2012), Sentinel-3 slstr active fire detection and frp product: Pre-launch algorithm development and performance evaluation using modis and aster datasets, *Remote Sensing of Environment*, *120*(0), 236 – 254, doi:10.1016/j.rse.2011.09.033.

Zhukov, B., E. Lorenz, D. Oertel, M. Wooster, and G. Roberts (2005), Spaceborne detection and characterization of fires during the bi-spectral infrared detection (bird) experimental small satellite mission 2001-2004, *Remote Sensing of Environment*, *100*, 2951.

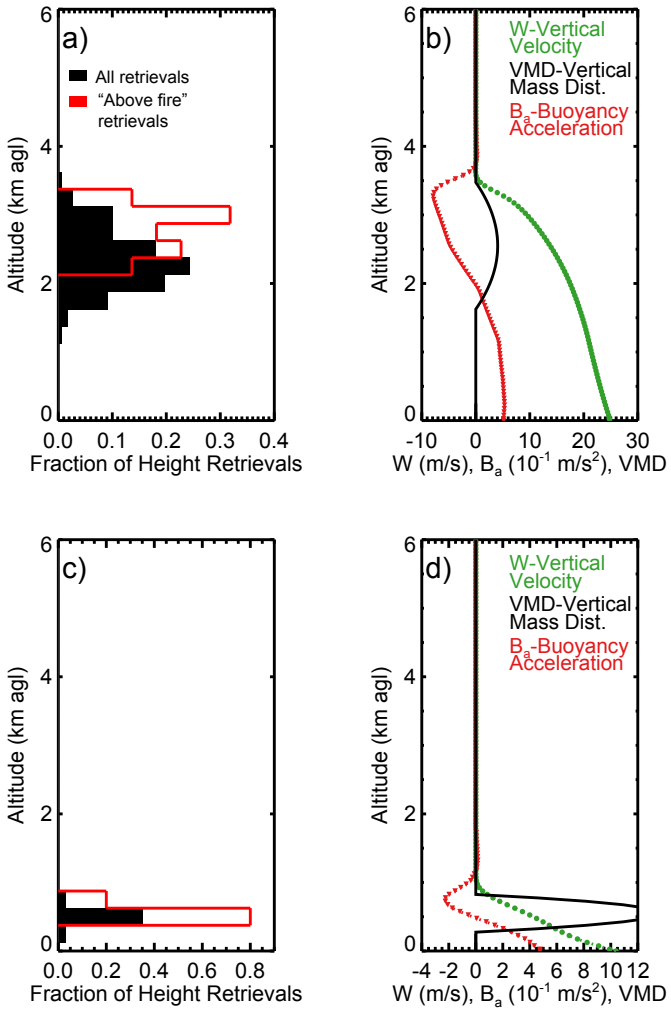

Figure 1. Example of the vertical distribution of MISR stereo-height pixels for a boreal forest fire in central Canada (a) and a grassland fire in Texas (c). Also shown are 1-D plume-rise model outputs obtained for the forest fire with heat flux of 120 kW/m^2 and area of 127 ha (b), and for the grassland fire with heat flux of 55 kW/m^2 and fire area of 3.5 ha (c).

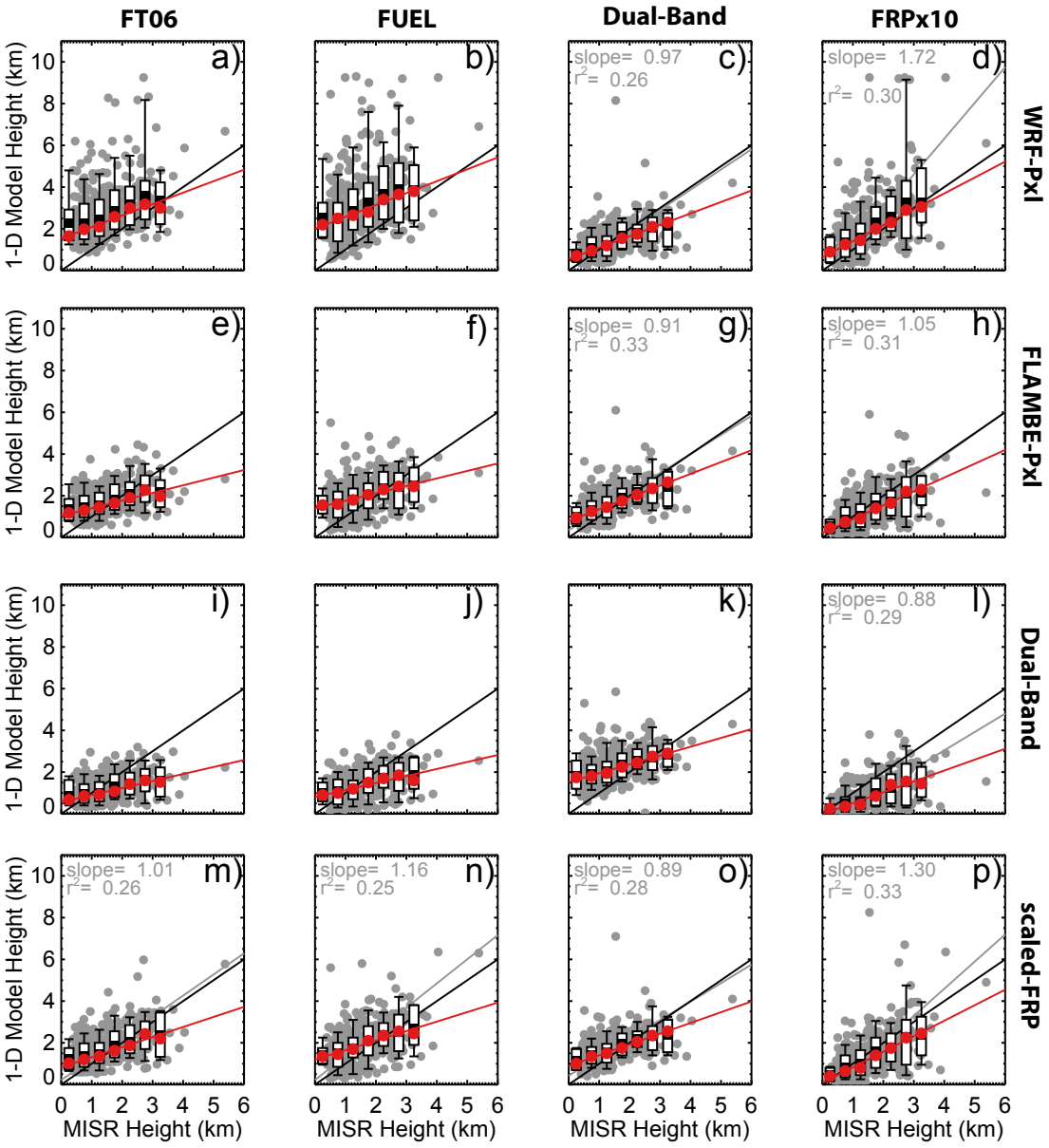

Caption included in next page

Figure 2. Relationship between MISR observed maximum plume heights and 1-D plume-rise model simulated plume heights for the active fire area configurations (a)-(d) WRF-Pxl, (e)-(h) FLAMBE-Pxl, (i)-(l) Dual-Band and (m)-(p) scaled-FRP, and the total heat flux configurations (a),(e), (i) and (m) FT06, (b), (f), (j), (n) FUEL, (c), (g), (k), (o) Dual-Band and (d), (h), (l), (p) FRPx10. See table 2 and text for explanation. Regression lines for correlations with r^2 below 0.25 are not shown. Grey lines are the two-sided regression line [*Ayers*, 2001]; black line is the 1:1 relationship. Bar plots are the distributions of model heights and 500-m resolution MISR heights. The medians (red circles) are shown along with the central 67% (box) and the central 90% (thin black lines). Red lines are the regression line of the distribution medians.

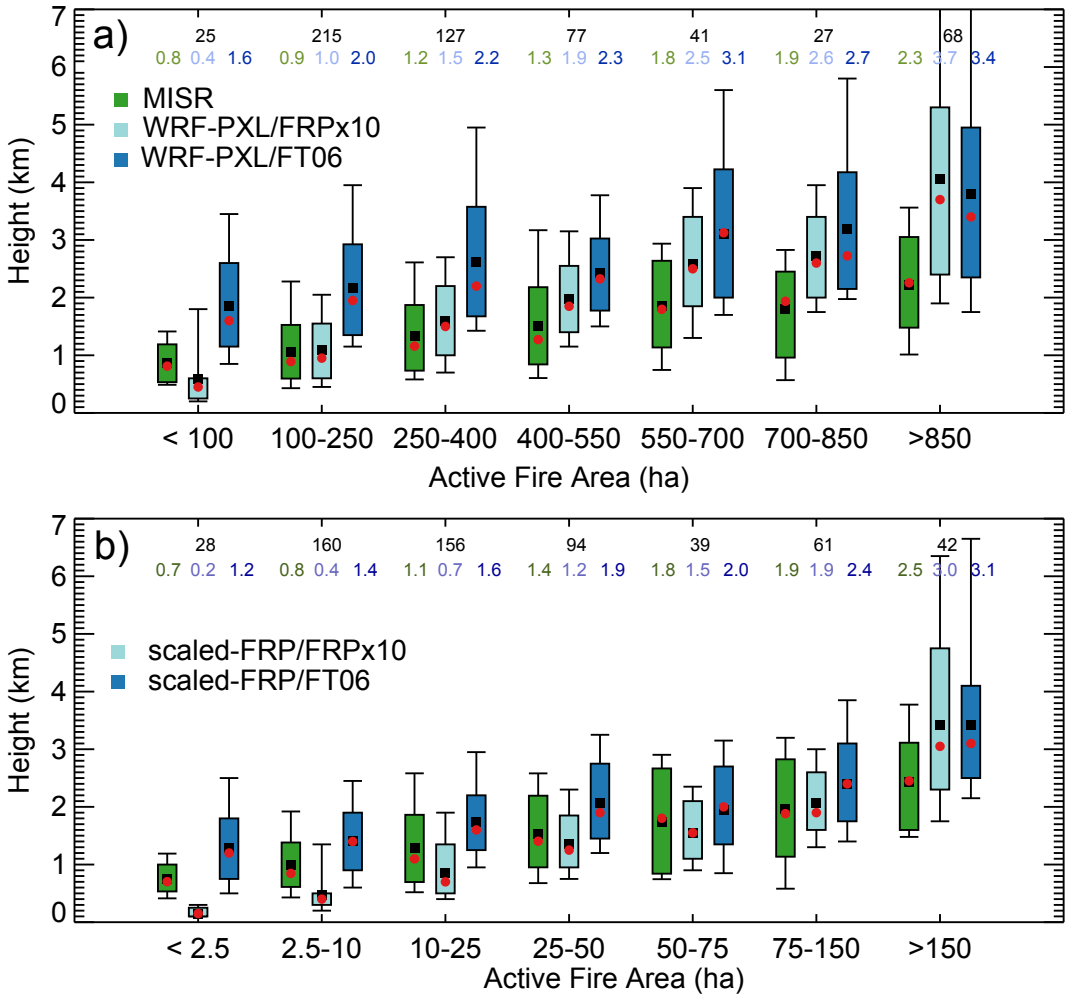

Figure 3. Distribution of the MISR plume height (green) and the 1-D plume-rise model height for (a) WRF-Pxl/FT06 (blue) and WRF-Pxl/FRPx10 (light blue) and (b) scaled-FRP/FT06 (blue) and scaled-FRP/FRPx10 (light blue) configurations grouped by active fire area. The medians (red circles) and the means (black squares) are shown along with the central 67% (blue, light blue or green) and the central 90% (thin black lines). The number of observations (in black) and the median heights (in colors) included in each distribution are given at the top of the plot.

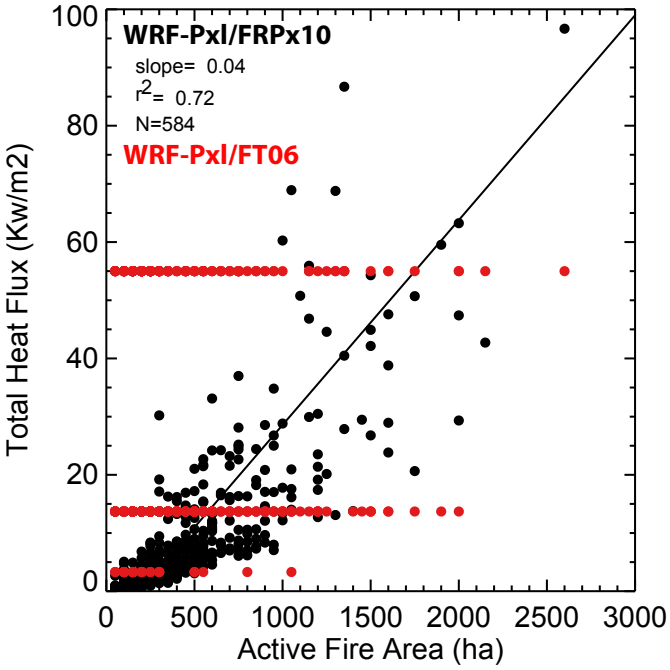

Figure 4. Relationship between active fire area and total heat flux for WRF-Pxl/FT06 (in red) and WRF-Pxl/FRPx10 (in black). Black line is the two-sided regression line for WRF-Pxl/FRPx10.

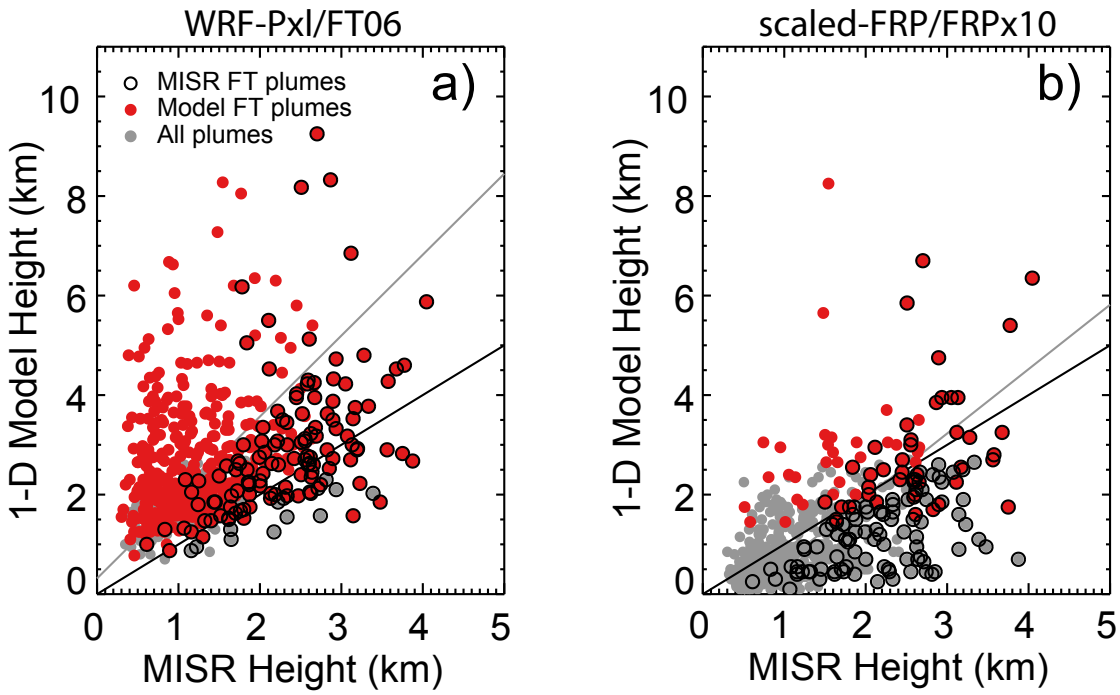

Figure 5. Relationship between MISR plume height and the plume-rise model height for WRF-Pxl/FT06 (a) and scaled-FRP/FRPx10 (b) configurations. All observations are shown in grey, plumes located in the FT by the model are shown in red, and plumes in the FT by MISR are shown with open black circles; black line is the 1:1 relationship.

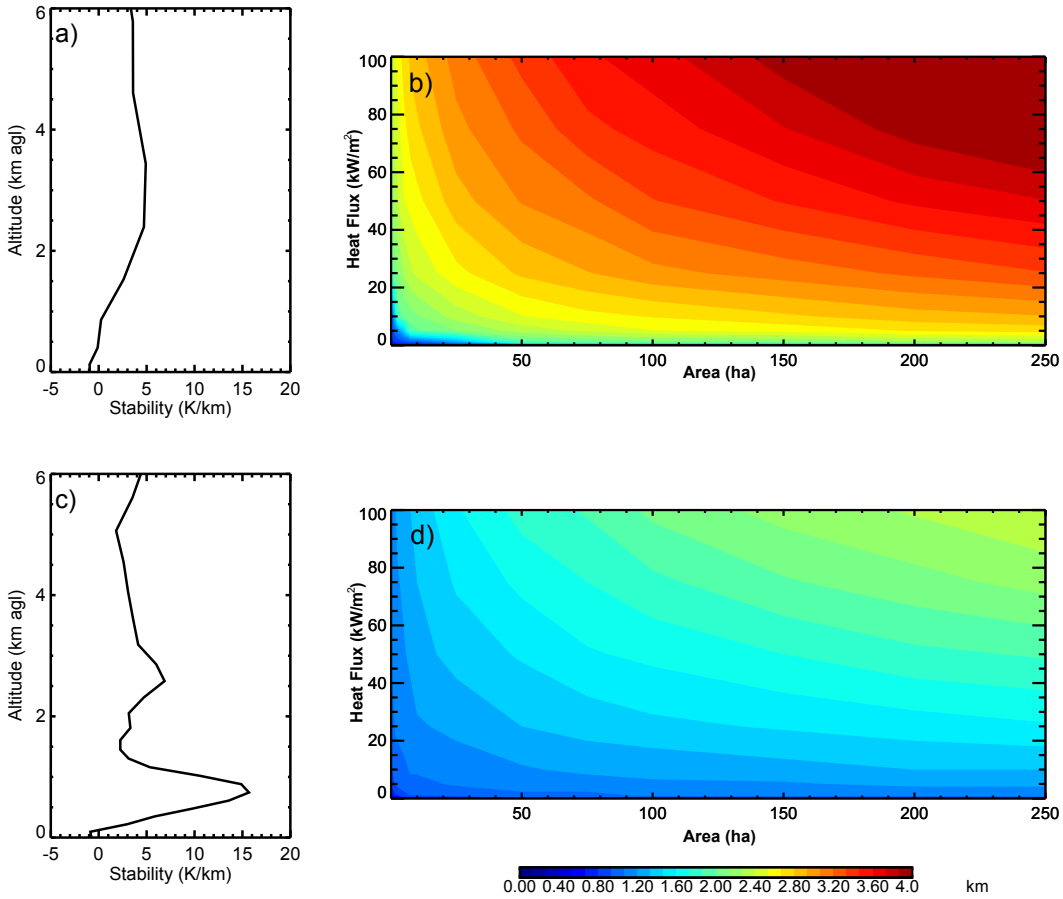

Figure 6. Atmospheric stability profiles for the MISR plumes shown in Figure 1a (a) and Figure 1b (c), and the associated contour plots for the injection height as a function of fire area and total heat flux simulated by the model (b and d)

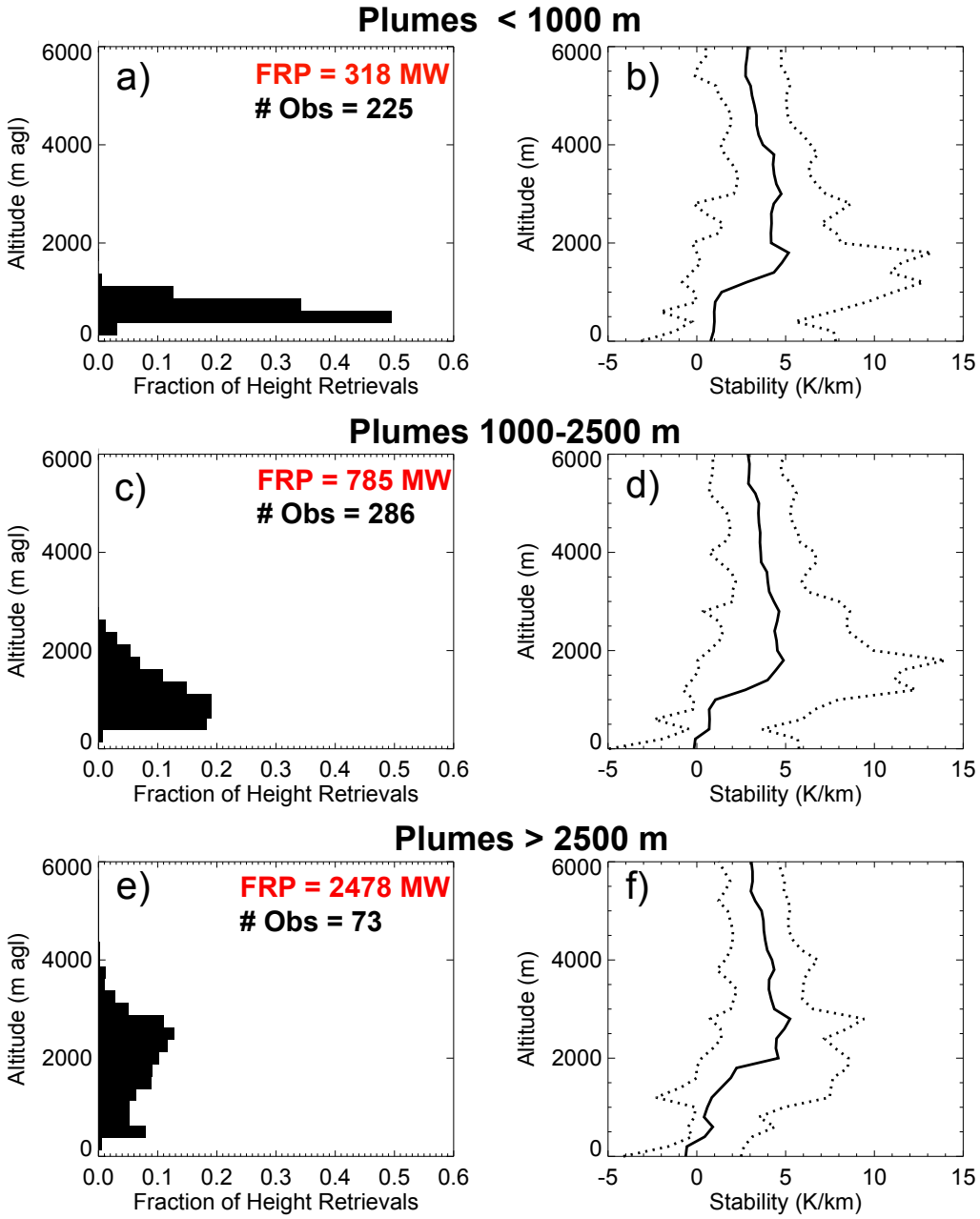

Caption included in next page

Figure 7. Vertical distribution of the MISR stereo-height retrievals for the 584 plumes analyzed, classified as low altitude plumes (a), medium altitude plumes (c) and high altitude plumes (e). The atmospheric stability structures associated with this classification (b, d, f) are shown as the median (solid line) and the 5th and 90th percentiles (dotted lines). Numerals in red and black indicate the mean of the MODIS FRP and the number of plumes in each distribution, respectively.

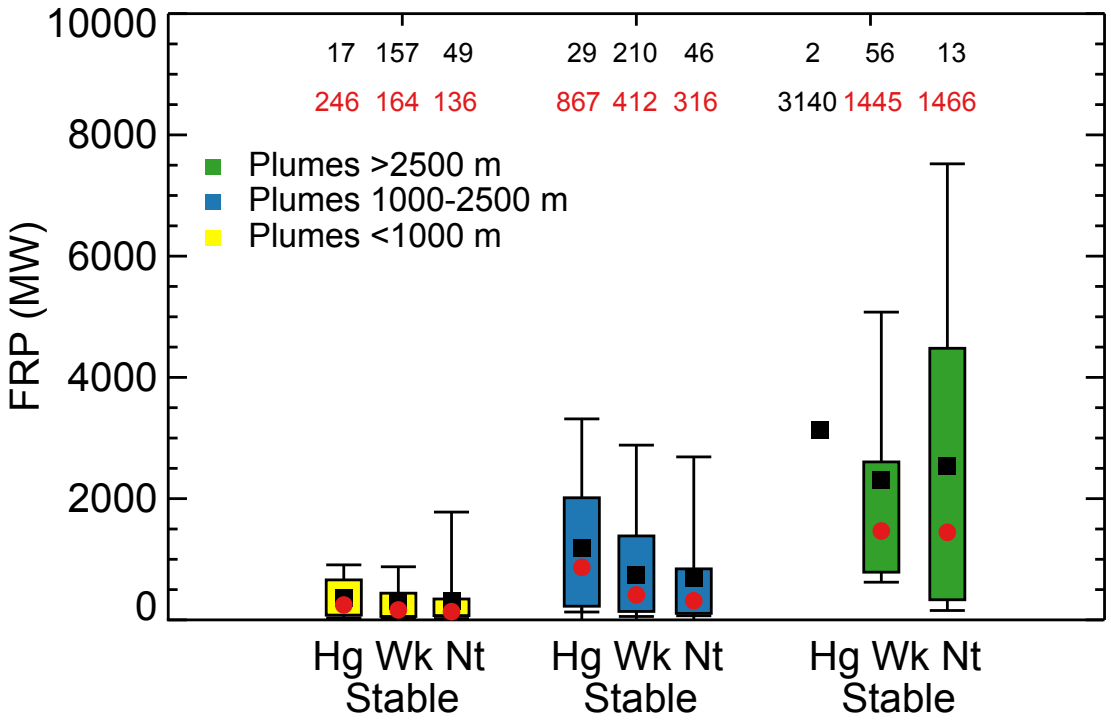

Figure 8. Distribution of MODIS FRP by atmospheric stability (Hg=highly, Wk=weakly and Nt =neutrally) for plumes below 1000 m (yellow), plumes between 1000-2500 m (blue) and plumes above 2500 m (green). (See text for further explanation). The medians (red circles) and the means (black squares) are shown along with the central 67% (in color) and the central 90% (thin black lines). The number of observations (in black) and the median heights (in colors) included in each distribution are given at the top of the plot. A distribution with 2 plumes is shown as the average (black square).

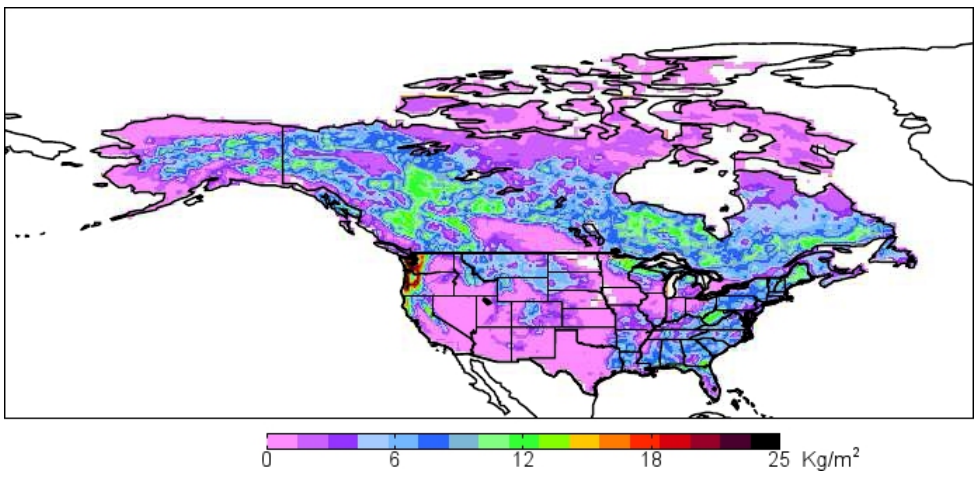

Figure 9. Fuel consumption (in kg dry matter/m^2) map for North America for moderately-dry fuel moisture conditions in the boreal region.

Table 1. 1-D Plume-rise models used for smoke injection height simulations.

Plume-rise Parameterization	Scheme	Hosted Model
Briggs [1969]	Empirical	CMAQ[a]
		HYSPLIT[b]
Lavoue et al. [2000]	Empirical	
Kahn et al. [2007]	Physical	
	(diagnostic)	
Achtemeier et al. [2011]	Empirical	CMAQ[c]
Freitas et al. [2007, 2010]	Physical	CATT-BRAMS[d]
	(prognostic)	NCAR-CAM[e]
		FLEXPART[f]
		WRF-Chem[g]
Rio et al. [2010]	Physical	LMDZ
	(prognostic)	
Sofiev et al. [2012]	Empirical	

[a] *Raffuse et al.* [2012]; [b] *Stein et al.* [2009]; [c] *Achtemeier et al.* [2011] and *Liu et al.* [2010];[d] *Freitas et al.* [2007]; [e] *Guan et al.* [2008];[f] *Brioude et al.* [2009]; [g] *Pfister et al.* [2011], *Grell et al.* [2011] and *Sessions et al.* [2011]

Table 2. Summary of the configurations based on active fire area and total heat flux parameters.

Active Fire		Total Heat Flux		
Area	*Freitas et al.*,[2006]	Fuel Consumption	Dual Band	FRPx10
WRF-Chem Pixel	WRF-Pxl/FT06	WRF-Pxl/FUEL	WRF-Pxl/Dual-Band	WRF-Pxl/FRPx10
FLAMBE Pixel	FLAMBE-Pxl/FT06	FLAMBE-Pxl/FUEL	FLAMBE-Pxl/Dual-Band	FLAMBE-Pxl/FRPx10
Scaled FRP	scaled-FRP/FT06	scaled-FRP/FUEL	scaled-FRP/Dual-Band	scaled-FRP/FRPx10
Dual Band	Dual-Band/FT06	Dual-Band/FUEL	Dual-Band/Sent3	Dual-Band/FRPx10

Table 3. Summary of the active fire area and total heat flux for each biome[a].

Configuration	Biome Type Forest	Shrubland	Grassland-Crop
	Fire Size (ha)		
WRF-Pxl	445 ± 467 (250)	410 ± 375 (250)	230 ± 208 (150)
FLAMBE-Pxl	45 ± 47 (25)	41 ± 38 (25)	23 ± 21 (15)
scaled-FRP	61 ± 101 (20)	44 ± 81 (18)	20 ± 25 (8)
Dual-Band	8 ± 15 (3)	6 ± 11 (3)	2 ± 3 (15)
	Heat Flux (kW/m^2)		
FT06[b]	30-80	4.4-23	3.3
FUEL	48 ± 30 (52)	36 ± 24 (38)	32 ± 27 (40)
FRPx10	10 ± 16 (3)	7 ± 13 (3)	3 ± 4 (2)
Dual-Band	23 ± 19 (18)	18 ± 14 (14)	20 ± 19 (14)

[a]Reported are mean, standard deviation (SD) and median, as Mean±SD (Median).

[b]Shown upper and lower limit values from *Freitas et al.* [2006].

Table 4. Statistical summary of the parameters shown in Figure 7 for all observations and for each biome[a].

Plume	FRP (MW)		Stability		N
Height[b]	Mean±SD	Median	Stable layer (K/km)	Altitude (m)	
			All Observations		
Low	318 ±485	164	5.3-13.2	1800	225
Medium	785 ±997	409	5.4-14.0	1800	286
High	2478±3070	1450	5.1-9.4	2800	73
			Forest		
Low	**428 ±672**	**226**	**4.8-13.6**	**1200**	**81**
Medium	**948 ±1230**	**409**	**5.5-14.7**	**1800**	**86**
High	3032±3130	2170	4.8-12.1	2300	29
			Shurbland		
Low	**259 ±326**	**147**	**5.7-12.6**	**1800**	**126**
Medium	**744 ±899**	**425**	**5.3-11.4**	**1800**	**182**
High	2250±3170	1370	5.2-9.4	2800	39
			Grassland-Crops		
Low	177 ±192	136	5.7-13.2	1700	17
Medium	377 ±437	239	5.8-14.6	1800	17
High	882 ±775	957	9.2-13.1	2800	3

[a]For FRP, mean, standard deviation (SD) and median are reported; for stability, the median and the 90th percentile of the absolute stability, and the altitude of the stable layer are reported; N is number of observations. Results for each biome with more than 50 data points are shown bold-faced.

[b]Plume heights are "low" for plumes<1000 m, "medium" for plumes between 1000 and 2500 m and "high" for plumes>2500 m (see text for explanation).

Table 5. Conversion of the Canadian Fire Behavior Prediction (FBP) fuelbeds into the U.S. Fuel Characteristic Classification System (FCCS) fueldbeds.

FBP		FCCS	
Code	Fuelbed name	Code	Fuelbed Name
		Canada	
C1	Spruce-lichen woodland	85	Black spruce / lichen forest
C2	Boreal spruce	87	Black spruce / feathermoss
C3	Mature jack or lodgepole pine	146	Jack pine forest
C4	Immature jack or lodgepole pine	148	Jack pine forest (wildfire)
C5	Red and white pine	138	Red pine-eastern white pine forest
C6	Conifer plantation	4	Douglas-fir / ceanothus forest
C7	Ponderosa pine / Douglas-fir	67	Interior ponderosa pine - Douglas-fir forest
D1	Leafless aspen	142	Trembling aspen - paper birch forest
M1, M2	Boreal mixedwood	92	Aspen/paper birch/white spruce/black spruce forest
O1	Grassland	99	Bluejoint reedgrass grassland
Tundra-Alpine	Tundra	97	Cottongrass grassland
		Alaska	
C2	Boreal spruce	87	Black spruce/ feathermoss
M1, M2	Boreal mixedwood	92	Aspen/paper birch/white spruce/black spruce forest
O1a/O1b	Grassland	98	Marsh Labrador tea-Lingonberry tundra shrubland
O1	Grass, Standing Dead Grass	99	Bluejoint reedgrass grassland

Table 6. Fuelbed stratum moisture (in %) for each moisture category.

Moisture	Fuelbed Stratum		
Conditions	10-hr	1000-hr	duff
Extra-Dry	6	8	25
Dry	8	12	40
Moderately-Dry	9	15	70
Moist	12	22	150
Wet	20	31	250

Table 7. Summary of the fuel consumption values (in kg/m^2) by fuelbed and fuel moisture content conditions.

Fuelbed	Extra-Dry	Dry	Moderately-Dry	Moist	Wet
C1	6.73	6.01	4.40	1.19	1.08
C2	15.15	14.02	11.53	4.41	2.18
C3	15.00	14.95	14.80	13.90	9.31
C4	5.61	5.41	5.07	4.70	4.26
C5	14.97	14.79	14.41	12.89	7.04
C6	8.90	8.27	7.00	5.74	3.56
C7	5.21	4.93	4.46	3.87	3.68
D1	8.78	8.40	7.30	4.36	4.08
M1-M2	4.31	3.80	3.18	2.90	2.77
O1	2.36	2.07	1.44	1.25	1.13
O1a/O1b	1.25	0.85	0.40	0.40	0.34
Tundra	3.62	1.65	1.62	1.26	0.91